Solid Earth Discuss., doi:10.5194/se-2017-11, 2017
Manuscript under review for journal Solid Earth
Published: 7 February 2017

SWITCHING DEFORMATION MODE AND MECHANISMS DURING SUBDUCTION OF CONTINENTAL CRUST: A CASE STUDY FROM ALPINE CORSICA

Giancarlo Molli [a], Luca Menegon [b], Alessandro Malasoma [c]

a Dipartimento di Scienze della Terra, Università di Pisa, Via S. Maria, 53, Pisa 56126, Italy

b School of Geography, Earth and Environmental Sciences, Plymouth University, Plymouth, UK

c TLS Lab and Geoservices, Via Vecchia Fiorentina, 10, 56023 Cascina, Pisa Italy

Correspondence to: Giancarlo Molli (giancarlo.molli@unipi.it)

Abstract. The switching in deformation mode (from distributed to localized) and mechanisms (viscous versus frictional) represent a relevant issue in the frame of crustal deformation, being also connected with the concept of the brittle-"ductile" transition and seismogenesis. In subduction environment, switching in deformation mode and mechanisms may be inferred along the subduction interface, in a transition zone between the highly coupled (seismogenic zone) and decoupled deeper aseismic domain (stable slip). On the other hand, the role of brittle precursors in nucleating crystal-plastic shear zones has received more and more consideration being now recognized as fundamental in the localization of deformation and shear zone development, thus representing a case in which switching deformation mode and mechanisms interact and relate to each other. This contribution analyzes an example of a crystal plastic shear zone localized by brittle precursor formed within a host granitic-protomylonite during deformation in subduction-related environment. The studied structures, possibly formed by transient instability associated with fluctuations of pore fluid pressure and episodic strain rate variations may be considered as a small scale example of fault behaviour associated with a cycle of interseismic creep and coseismic rupture or a new analogue for episodic tremors and slow slip structures. Our case-study represents, therefore, a fossil example of association of fault structures related with stick-slip strain accomodation during subduction of continental crust.

1. Introduction

The study of deformation fabric of fault rocks has been the base to develop a general model for crustal scale fault zones (Sibson, 1977; Sibson, 1983; Scholz, 1988; Scholtz, 2002; Handy et al., 2007; Cooper et al. 2010; Platt and Behr, 2011). In this model, the increasing PT conditions determine the transition from a seismogenic frictional regime, dominated by pressure-sensitive deformation and involving cataclasis and frictional sliding, to a viscous regime (Rutter, 1986; Schimd and Handy, 1991; Handy and Brun, 2004), where dominantly aseismic, mainly crystal-plastic and continuous shearing is localized within mylonitic shear zones. In quartzo-feldspathic rocks, this transition is primarily determined by temperature-related quartz response to change in deviatoric stress, with dislocation creep becoming the principal deformation mechanism at T>270 °C (Stipp et al., 2002 and references).

Rock deformation experiments (Rutter, 1986; Shimamoto and Logan 1986; Bos and Spiers 2002; Scholz 2002) have shown that the shear strength of simulated faults at the brittle-viscous transition may depend on normal stress (as by faulting dominated by cataclastic mechanisms) although strain is achieved through crystal plasticity and/or solution transfer. These results support the hypothesis that some mylonitic shear zones are produced by coupled frictional and viscous mechanisms under semi-brittle conditions (Shimamoto and Logan, 1986; Shimamoto, 1989; Chester, 1989; Scholz, 2002; Pec et al., 2012 and references). Studies on semi-brittle behaviour leave several open questions regarding natural fault zones including micromechanisms controlling bulk-rock deformation, the degree of interdependence of active deformation mechanisms, their cyclicity and the associated bulk rock style of deformation (Sibson, 1980; White and White, 1983; Takagi et al., 2000; Handy and Brun, 2004; Pec et al., 2012). Complex transitional behaviour involving mixed continuous and discontinuous, distributed vs. localized, and cyclic switching in deformation mechanisms over large variations in strain rates is inferred at the transition between frictional and viscous domains, a zone which includes the typical hypocentres and rupture depths for large earthquakes in continental crust (Sibson, 1983; Kohlstedt et al., 1995; Scholz, 2002; Handy and Brun, 2004).

In convergent subduction settings, similarly, the transition zone, located between 10 and 35 km depth depending on slab dip and thermal structure (i.e., between temperatures of 150 °C and 350–450 °C), along subduction interfaces is recognized as the site of megathrust earthquake nucleation and concentrated postseismic afterslip, as well as the focus site of episodic tremor and slow slip events (Hacker et al., 2003; Vannucchi et al., 2008; Meneghini et al., 2010; Angiboust et al., 2012; Andersen et al., 2014; Hayman and Lavier, 2014; Fagereng et al., 2014; Angiboust et al., 2015).

The feedback between brittle and viscous deformation modes is relevant also for the mechanisms of shear zone nucleation, so that fracturing has been proposed to be even a pre-requisite for the initiation of ductile shear zones in the lithosphere (Handy and Stünitz, 2002; Pennacchioni and Mancktelow, 2007; Fusseis and Handy, 2008, among others). Shear zones and style of strain accommodation in terms of distributed vs. localized deformation in granitoids have been described by different authors (Ramsay and Graham, 1970; Burg and Laurent 1978; Simpson, 1983; Gapais et al. 1987; Goncalves et al., 2016 and references therein). In this context, the role of brittle precursors in nucleating crystal-plastic shear zones has received more and more consideration being now recognized as having a fundamental role in the localization process (Segall and Simpson, 1986; Mancktelow and Pennacchioni, 2005; Pennacchioni, 2005; Pennacchioni and Mancktelow, 2007; Menegon and Pennacchioni, 2010; Pennacchioni and Zucchi 2012, among others).

However these works mostly deal with brittle precursors consisting of inherited structures such as discontinuities already existing at the beginning of deformation, as the cases of cooling joints, cataclasites and veins (e.g. Guermani and Pennacchioni, 1998; Pennacchioni and Mancktelow 2007) and most of them consider deformation at shallow to intermediate crustal depths (Fusseis and Handy, 2008; Mazzoli et al., 2009; Molli et al., 2011) although case studies framed under conditions of upper amphibolite to granulite facies (White, 1996; Pennacchioni and Cesare, 1997; Kisters et al., 2000; Pittarello et al., 2013; Altenberger et al., 2013) and eclogite facies (Austrheim and Boundy, 1994; Austrheim, 2013 and references therein) were also investigated.

The case of deformation of crustal units and granitoids during subduction has been only recently analysed in terms of rock records of paleo-seismic cycle and/or slow-slip phenomena (Angiboust et al., 2015). A well-documented study from the Dent Blanche Thrust in the Western Alps is framed in the hangingwall of an ancient subduction interface zone (Angiboust et al., 2014; 2015). On the contrary, our contribution analyses a microscale example of brittle precursor of a crystal plastic shear zone derived from the footwall of a subduction interface in ambient blueschist-facies conditions thus representing a still not yet or less documented case study (Molli et al., 2005; Molli 2007).

By virtue of their deep origin, the analysed structures are ideally suited to contribute to the ongoing discussion on the deformation style and mechanisms associated with the broad spectrum of fault-slip behaviour (from seismic slip to stable aseismic creep, to episodic slow slip events and non-volcanic tremors) recorded by seismic and geodetic observations at active plate boundaries (e.g. Peng and Gomberg 2010; Beroza and Ide, 2011, and references therein). Slow slip events (i.e. fault slip events with slip rates in between coseismic slip and aseismic creep, and generating equivalent seismic moments similar to large earthquakes) in subduction zones have been recorded in a depth interval that experiences temperatures between 250 and 650° C and pressures between 0.6 and 1.2 GPa (Beroza and Ide, 2011), typically in areas of high Vp/Vs ratios suggestive of local high fluid pressures. This locates slow slip events at the lower end of the seismogenic zone, at metamorphic conditions where the rheology is expected to be viscous or at the frictional-viscous transition. Accordingly, recent studies of

Solid Earth Discuss., doi:10.5194/se-2017-11, 2017
Manuscript under review for journal Solid Earth
Published: 7 February 2017

shear zones exhumed from similar conditions along the subduction interface have suggested that coupled fracture and viscous flow, possibly associated with fluctuations in fluid pressure, can originate tremors and slow slips (e.g. Fagereng et al., 2014; Hayman and Lavier, 2014; Angiboust et al., 2015; Malatesta et al., 2017). Here we show that the HP brittle-viscous transition preserved in the Popolasca granitoids can also be explained with transient high fluid pressures triggering brittle deformation in an otherwise viscous regime, and discuss the related implications for fault-slip behaviours in subduction zones.

2. Regional background and Geological Setting of studied sample

In Alpine-type orogens the study of meso- and microstructural record of exhumed subduction related thrust zones and its interpretation in terms of subduction zone rheology and seismicity have received increasing attention since the end of ’90 (Stöckhert et al.,1999; Kuster and Stöckhert, 1999). This subject has been developed in particular in the Alpine Corsica (Austrheim and Andersen, 2004; Andersen and Austrheim, 2006; Healy et al., 2009; Andersen et al., 2014; Deseta et al., 2014a,b; Magott et al., 2016a,b) in oceanic units made up of peridotite, serpentinite, gabbro, basalt, calcareous and siliceous schist and marble exposed as remnants of the lithosphere of the Jurassic Piemonte- Liguria oceanic basin and its pelagic sedimentary cover (Mattauer et al., 1981; Bezert and Caby, 1988; Jolivet et al., 1990; Molli, 2008; Vitale Brovarone et al., 2013).

These widespread occurrences and preservations of relicts of seismogenic exhumed structures are mainly related to the peculiar geologic history of Alpine Corsica, connected with the development of the Alps/Apennine orogenic system (Molli and Malavieille, 2011; Guyedan et al., 2017; Beaudoin et al., in press) with the lacks of the continent-continent “hard collision”- related structures and thermal reworking observable in the Alps (e.g. Polino et al., 1995; Schmid et al., 1997; Berger and Busquet, 2008; Butler, 2013; Rosenberg and Kissling, 2013; Carminati and Doglioni, 2014) and a better preservation of the early stages of subduction-related structures and fabrics.

Corsica, therefore, represents a suitable natural laboratory for the investigation of the subduction-related processes in oceanic and continental crust as firstly suggested by Mattauer et al. (1981) and Gibson and Horak (1984).

In Corsica, continental-derived units, i.e. units derived from the footwall of ancient subduction interface zone, can be observed in three different structural positions (Fig.1), each of them corresponding to a different peak metamorphism (Tribuzio and Giacomini, 2004; Molli, 2008; Vitale Brovarone et al., 2013):

- the innermost slices (Serra di Pigno/Farinole units) interleaved with oceanic units show eclogite peak conditions at 1,5/1,8 GPa; 500 ± 50 °C;

- the intermediate ones (e.g. the Tenda and Centuri units) are instead characterized by Upper Blueschist facies peak conditions at 0,9/1,1 GPa; 450± 50 °C;
- the most external (e.g. Corte/Popolasca units) show high pressure greenschist and/or blueschist facies peak assemblages developed at T =325/370°C, P = 0.75/0.85 GPa (Malasoma et al., 2006; Di Rosa et al., 2016).

These occurrences document the progressive underthrusting at different depths and their in-sequence contractional exhumation within an alpine-age east-dipping subduction system (Mattauer et al., 1981; Bezert and Caby, 1988; Jolivet et al., 1990; Garfagnoli et al., 2009; Molli and Malavieille, 2011; Maggi et al., 2012; Di Rosa et al., 2016; Guyedan et al., 2017).

The studied samples come from the external continental units (Molli, 2008; Molli and Malavieille, 2011; Vitale Brovarone et al., 2013) of Alpine Corsica and in more detail from the Popolasca Unit (Bezert and Caby, 1988; Malasoma et al., 2006; Di Rosa et al., 2016). This unit is characterized by a pre-Mesozoic basement mainly formed by granitoids, a Permo-Mesozoic metasedimentary sequence and an Early-Eocene flysch (Fig. 1).

Blueschist assemblages in the unit have been described by regional studies (Bezert and Caby, 1988; Malasoma et al., 2006; Molli, 2008; Di Rosa et al., 2016) and can be observed in all suitable rock-types: in metapelites from cover rocks, in metabasic dykes and some of the granitoid suites from the basement. Peak metamorphism has been constrained at 250/350°C, 0.4/0.55 GPa (Bezert and Caby, 1988) or more recently better defined at 325/370 °C and 0.75/0.85 GPa (Malasoma et al., 2006; Di Rosa et al., 2016). The prograde to peak pressure assemblage has been recently dated in the range of 45-36 Ma by Di Vincenzo et al., (2016).

The contributions of Malasoma et al., (2006), Di Rosa et al., (2016) analysed the cartographic to mesoscopic-scale structural geometries of deformation in the area of the studied sample.

Superimposed foliations and fold structures are typical of the metasedimentary cover, with blueschist assemblages as relict fabrics. On the contrary, in basement rocks a main phase continuous foliation can be observed wrapping around undeformed granitoids. The main foliation is either associated with blueschist or greenschist facies assemblages (Malasoma et al., 2005; Di Rosa et al., 2016; Di Vincenzo et al., 2016). Anastomosed network of fault zones associated with subgreenschist facies assemblages overprints all previous structures and may be related to the activity of a major N/S trending transcurrent fault zone (Central Corsica Fault Zone) reworked by normal kinematics active during Oligocene-Miocene in the frame of rototranslation of Corsica-Sardinia microblock and upper-plate extension associated with Apenninic subduction (Faccenna et al., 2004; Molli, 2008; Molli and Malavieille, 2011; Carminati and Doglioni, 2014; Guyedan et al, 2017).

3. Geometry of deformation and microstructures

The analysed sample (Fig.2) is a deformed granitoid of calcalcaline suite (K-feldspar, plagioclase, quartz, biotite) well known in the Hercynian Corsica (Rossi et al., 2001). It shows a continuous foliation (Fig.2,3a,b) mainly defined by the shape preferred orientation of quartz, feldspars and biotite grains.

Shape anisotropy of quartz in the host protomylonite shows an aspect ratio around 0,37 (mean X/Z of 2,7) which indicates a shear strain γ of c.1 assuming deformation in simple shear.

Quartz shows typical features of low temperature plasticity (Tullis et al., 2000; Stipp et al., 2002; Vernooij et al., 2006; Trepmann et al., 2007; Derez et al., 2015; Kjøll et al., 2015) (Fig 3), such as undulatory extinction, localized extinction bands (LEBs, following the terminology of Derez et al., 2015), typically forming conjugate sets, and up to 100 μm thick intracrystalline bands of recrystallized grains (5-10 μm in size). Bands of recrystallized grains occur parallel to the main foliation as well as in conjugate sets intersecting at ca. 90° and parallel to the conjugate sets of LEBs.

Feldspars show local evidence of grain size reduction by microcraking and microfaulting (Fig.3) associated with K-feldspar breakdown to albite (by bulging recrystallization) (Fig.3), stilpnomelane and phengite. Thin needles of Na-amphibole (Fig.4) attest the development of this fabric in HP/LT conditions as described below.

The main foliation is cross-cut at high angle by a millimetre-thick localized zone of deformation (Fig.2,5). This shows a sharp boundary, truncating flattened quartz and feldspar grains; a feature suggesting its development as unstable fracture (Schmid and Handy, 1991; Passchier and Trouw, 2011). Three compositionally controlled domains can be recognized within the thin localized shear zone (Fig.2,5):

Domain 1 is feldspar-dominated and shows microstructural features typical of a cataclasite (Fig.5a,c). Feldspar clasts (and quartz grains) reveal both displacive intragranular fractures and intergranular "stable" cracks (Atkinson, 1982; Schmid and Handy, 1991).

Domain 2 is "phyllosilicate"-dominated (stilpnomelane and phengite) and shows microstructural features of a foliated-cataclasite/phyllonite (Fig.5a,b). Asymmetric porphyroclasts and shear band systems characterize the phyllosilicate-rich parts of the shear zone.

Domain 3 is a quartz-albite rich domain showing microstructural features typical of an ultramylonite. This is characterized by very fine recrystallized albite and quartz grains (5-10 μm in size) (Fig.5a,b; Fig.6) with strong crystallographic preferred orientation (see below). Quartz porphyroclast shows a mean aspect ratio around 0,09 (mean X/Z of 11) which corresponds to a calculated shear strain γ of c. 3

At this shear strain the corresponding angle between the foliation and the shear zone boundary in simple shear is around 15 ° which agrees with the mean orientation of the quartz porphyroclasts shape preferred orientation defining the ultramylonitic foliation (Fig.6a,b,c) Syn to post-kinematic Na-amphibole (Fig.6a) documents shearing in HP/LT metamorphic conditions, as illustrated here below.

4. Mineral chemistry and estimate of metamoprphic Pressure-Temperature (P-T) conditions

Chemical analyses of coexisting minerals within the metamorphic assemblage (Tab.1) were obtained using a JEOL JXA-8600 electron microprobe, equipped with four wavelength-dispersive spectrometers, at the CNR - Istituto di Geoscienze e Georisorse, Firenze, Italy. Running conditions were 15 kV accelerating voltage and 10 nA beam current on a Faraday cage. Counting time for the determined elements ranged from 10 to 60 s at both peak and background. The Bence and Albee (1968) method was employed for the correction of all data. A number of synthetic and mineral standards were used for instrumental calibration.

Amphibole. Structural formulae were calculated assuming 23 oxygens, and the classification of Leake et al. (1997) was adopted. Site assignment and ferric iron contents were calculated using the scheme proposed by Schumacher in Leake et al. (1997). Because of the small sizes of the crystals (widths *c.*10μm), it was not possible to make compositional traverses across individual crystals to detect intracrystalline variations in chemical composition, such as core-to-rim zonation. Thus, each analysis reported in Table 1 represents a different crystal. In the studied sample the Na-amphiboles are mostly riebeckite (Tab.1 and Fig. 4b) with low Mg/(Mg+Fe2+) ratio (0.13-0.21) and are characterized by Si contents close to the maximum of 8.0 apfu.

Other minerals. All analysed albites, of which structural formulae were calculated assuming 8 oxygens, have composition close to the pure end-member. Stilpnomelane structural formulae were calculated assuming 24 oxygens and all Fe as divalent (Fe2+). Stilpnomelanes have Fe amounts ranging from 1.86 to 2.91 apfu and Mg amounts ranging from 0.24 to 0.58 apfu. For K-feldspar and biotite porphyroclasts, structural formulae were calculated assuming respectively 8 and 22 oxygens. The analysed K-feldspars have composition close to the orthoclase pure end-member, with minor amounts of Na.

The peak metamorphic mineral assemblage is characterised by Na-amphibole + phengite + quartz + albite + stilpnomelane. Na-amphibole is a typical mineral related to the blueschist facies and is indicative of HP/LT gradient metamorphism (e.g. Evans 1990; Schiffman & Day 1999 and references). The minimum temperature (T) and pressure (P) conditions of this mineral assemblage can be estimated using the reaction curves proposed by Schiffman & Day (1999) for the appearance of Na-amphibole

Solid Earth Discuss., doi:10.5194/se-2017-11, 2017
Manuscript under review for journal Solid Earth
Published: 7 February 2017

Solid Earth Discussions

(stability field of the blueschist facies); meanwhile the maximum temperature (T) conditions were constrained by the presence of stilpnomelane, as shown by the equilibrium: Stp+Phe=Bt+Chl+Qtz+W (Massonne & Szpurka, 1997). Summing up all the available thermobarometric information, the metamorphic conditions can be estimated as temperature (T) around 320±50 °C and pressure (P) > of 0.70 GPa (Fig.4c); consistent with those described by Malasoma *et al.* (2006) in metagranitic rocks from the area of our studied sample.

5. EBSD data

EBSD analysis of quartz was conducted with a Jeol 7001 FEG-SEM equipped with a NordlysMax EBSD detector (Oxford Instruments) at the Plymouth University Electron Microscopy Centre. Working conditions during acquisition of the EBSD patterns were 20 kV, 70° sample tilt and high vacuum. Thin sections were chemically polished with colloidal silica and carbon-coated before the analysis. EBSD patterns were acquired on rectangular grids with step size of 1 μm and 2 μm. EBSD patterns were acquired and indexed with the AZtec software and processed with Channel 5 software (Oxford Instruments). Raw EBSD data were processed to reduce data noise following the procedure tested by Prior et al. (2002) and Bestmann and Prior (2003). EBSD results are shown in form of Inverse Pole Figure map, pole figures (equal angle, lower hemisphere) of crystallographic axes and planes (<0001> c-axis, <11-20> a-axis, {10-10} prism {m}, {10-11} positive rhomb {r}, {01-11} negative rhomb {z}), misorientation pofiles and plots of misorientation axis in sample coordinates.

5.1 Quartz in the host rock

We analysed a monocrystalline quartz ribbon elongated parallel to the host-rock foliation and sharply cut by the thin localized shear zone. The quartz ribbon contains two nearly orthogonal sets of intracrystalline shear bands of recrystallized grains (Fig. 7a); one set is oriented at high angle (90° ± 20, *set 1*) and one at low angle (≤ 20°, *set 2*) to the host rock foliation (vertical in Fig. 7a). The average grain size of the recrystallized grains is 5±2 μm. The ribbon contains also fine localized extinction bands (up to 20 μm thick) (LEBs: Derez et al., 2015) subparallel to the bands of recrystallized grains. Low-angle boundaries are ubiquitous in the ribbon; on EBSD maps they are typically straight, poorly connected, and subparallel to the bands of recrystallized grains (Fig. 7b). Some low-angle boundaries are connected to form subgrains of approximately the same size of the recrystallized grains. Subgrains occur with a higher frequency at the intersection between two sets of recrystallized bands, and in regions sandwiched between closely spaced (≤ 100 μm) subparallel bands of recrystallized grains (Fig.

Solid Earth Discuss., doi:10.5194/se-2017-11, 2017
Manuscript under review for journal Solid Earth
Published: 7 February 2017

Solid Earth Discussions Open Access EGU

7b).

The c-axis of the ribbon is oriented near the pole to the host-rock foliation, i.e. in a position suitably oriented for the activation of the basal <a> slip system of quartz (Fig. 7c). The c-axis orientation of the recrystallized grains in the intracrystalline bands is mostly spread out along the periphery of the pole figure, although some scattered grains have their c-axis in intermediate positions between the X and Y directions of the pole figures (Fig. 7d). Such an orientation suggests that the recrystallized grains have experienced a rotation around the Y-direction of finite strain (i.e. centre of the pole figure) from the host-grain orientation (e.g. Van Daalen et al., 1999; Menegon et al., 2011).

This is confirmed by the boundary trace analysis (Prior et al., 2002; Menegon et al., 2010) of the two main sets of straight low-angle boundaries defining localized extinction bands (parallel to bands of recrystallized grains), one running ENE-WSW (*subset1*) and one running ca. N-S (*subset 2*) in Fig. 7b. The dispersion paths of crystallographic directions on the pole figures of subset 1 (Fig. 7e) identifies {m} as the rotation axis, which lies very close to the centre of the pole figure. The pole to the prismatic plane {m} is the rotation axis associated with the basal <a> and with the {a} <c> slip system in quartz (e.g. Neumann, 2000), and, accordingly, subset 1 can be interpreted as a tilt boundary plane produced by the activity of the slip system basal <a> (Fig. 7e) and containing the boundary trace of subset 1 and the rotation axis.

Subset 2 has a similar dispersion path as subset 1, with {m} as the identified rotation axis. However, in this case the boundary trace analysis is not consistent with a tilt boundary produced by the activity of the slip system basal <a>, but could indicate the activity of the {a} <c> slip system (Fig. 7f). However, activity of c-slip in quartz typically requires temperature in excess of 600° C (Kruhl, 1996; Zibra et al., 2010) and, therefore, appears unlikely in our samples. Moreover, misorientation profiles across low angle boundaries with a subset 2 orientation show abrupt misorientation jumps of up to 6º (profiles 2 and 3 in Figs. 7b and 7g), as opposed to a gradual accumulation of misorientation towards low-angle boundaries with a subset 1 orientation (profile 1 in Figs. 7b and 7g). Thus, the low-angle boundaries with a subset 2 orientation could represent microcracks subparallel to the basal planes (e.g. Kjøll et al., 2015) that localized rigid body rotation of fragments around the Y-direction (e.g. Trepmann et al., 2007; Menegon et al., 2013). The rotation around Y of (1) the crystallographic directions of the host grain and (2) the recrystallized grains (in this case for large misorientation > 10°) is confirmed by the plots of the misorientation axis in sample coordinates (Fig. 2).

5.2 Quartz in the localized shear zone

We analysed polycrystalline ribbons of recrystallized grains from domain 3 of the localized shear zone (Fig. 8a). The c-axis orientation of the recrystallized grains defines an inclined type-I crossed girdle synthetically oriented with respect to the bulk shear sense of the shear zone (Fig. 8b). The c-axes are preferentially clustered near the pole to the shear zone boundary, i.e. in an orientation suitably oriented for the activity of the basal <a> slip system. The average grain size of the recrystallized grains in domain 3 is 6±2 μm.

6. Ultramylonite: Paleopiezometry, flow stress and strain rate

The microstructure and the crystallographic preferred orientation of quartz indicate that quartz in the protomylonite and ultramylonite deformed by dislocation creep (concomitant with microcracking in the protomylonite) and recrystallized to a fine-grained aggregate. Thus, the rheology and the flow stress in the ultramylonite can be evaluated extrapolating experimentally calibrated flow laws of quartz to the deformation conditions.

The rheology of quartz deforming by dislocation creep is generally described in terms of a power-law equation:

$$\dot{\varepsilon} = A f_{H_2O}^{m} e^{(-Q/RT)} \sigma^{n} \qquad (1)$$

Where $\dot{\epsilon}$ is the strain rate, f_{H2O} is the water fugacity (raised to the power of m), Q is the activation energy, R is the universal gas constant, T is the temperature, σ is the differential stress, and *n* is the stress exponent. We used the theoretical dislocation creep flow law of Hirth et al. (2001), which has derived a linear dependence of strain rate on the water fugacity (m=1) and a stress exponent of 4. A water fugacity of 172 MPa is calculated from the water fugacity coefficient reported in Tödheide (1972) at T=350° C, P=0.8 GPa.

The paleostress (assuming steady-state flow at time of viscous deformation) can be determined by recrystallized quartz grain size paleopiezometer (e.g. Stipp & Tullis, 2003), which have been calibrated in the form: $\Delta\sigma = B\, D^{-x}$,where Δσ is the steady state differential stress (σ1 - σ3), D is the recrystallized grain size and B and X are empirical constants. Using the recrystallized grain size piezometer of quartz calibrated by Stipp and Tullis (2003), a recrystallized grain size of 5-10 μm indicates differential stress in the range of 110-190 MPa. Extrapolation of the flow law of Hirth et al. (2001) yields a strain rate in the range of $7.6 * 10^{-13} – 6.2 * 10^{-12}$ sec^{-1} in the ultramylonite at the estimated deformation temperature of 350° C.

7. Discussion and conclusion

7.1 Viscous-brittle-viscous deformation under HP/LT conditions

Solid Earth Discuss., doi:10.5194/se-2017-11, 2017
Manuscript under review for journal Solid Earth
Published: 7 February 2017

The analysed example documents a switch in deformation mode and mechanisms within an HP/LT fault zone. On the base of overprinting relationships and microstructural features the following deformation sequence may be suggested: stage (1), associated with a distributed deformation and development of a protomylonitic foliation in the granitoid by quartz low temperature plasticity, microfracturing, and albite neo-crystallization from K-feldspar porphyroclasts (Fitzgerald and Stunitz, 1993), has been followed by stage (2), in which localized deformation by brittle fracturing formed a millimeter-thick cataclasite, which acted as a precursor for (3) localization of viscous deformation and ultramylonite development. The synkinematic and postkinematic growth of Na-amphibole in the host rock foliation and in localized ultramylonite indicates that the entire deformation sequence occurred at HP/LT conditions (ca. 350°C at ≥ 0.7GPa), corresponding to a depth of 23-30 km in the subduction channel.

The estimated P, T conditions are consistent with low-T plasticity regime in quartz (Stipp et al., 2002; Derez et al., 2015 and refs therein). Accordingly, the deformation microstructures of quartz produced during stage (1) in the host rock appear to be the product of the competition between dislocation activity and fracturing. Localized extinction bands at high angle to the host rock foliation (subset 1 in Fig. 7b) are consistent with the activity of the basal <a> slip system, whereas localized extinction bands subparallel to the host-rock foliation (subset 2 in Fig. 7b) are interpreted as fractures subparallel to the basal plane, as previously observed by Kjøll et al. (2015). Some localized extinction bands (especially those with a subset 2 orientation, see Fig. 7b) contain isolated small new grains that are considerably smaller than the average grain size in the recrystallized bands, and that are only slightly misoriented with respect to the host grain. Moreover, the high-angle boundaries in such localized extinction bands are not always fully connected to define entire new grains. Together with the abrupt misorientation jumps (Fig. 7g), these observations further suggest that localized extinction bands with a subset 2 orientation represent fractured domains in which the fragments have rotated passively and sealed together, as proposed by e.g. Derez et al. (2015).

Despite the local fracturing of the host grain, deformation of the recrystallized grains in the conjugate intracrystalline bands involved dislocation activity, as indicated by the cluster of misorientation axis around the prism {m} for low misorientations (compare Fig. 7h with 7d). This is consistent with the local activity of the basal <a> slip system in the recrystallized bands, as also indicated by the CPO of the recrystallized grains in the bands at high angle to the host rock foliation (Fig. 7d).

The type-I crossed girdle c-axis CPO of quartz in the ultramylonite suggests the concomitant activity of basal <a>, rhomb <a> and prims <a> slip systems in the recrystallized ribbons (Fig. 8). The grain size of recrystallized quartz in the ultramylonites is in the same range (5-10 μm) as in the intracrystalline bands in the host rock. This suggests that 5-10 μm represents the equilibrium grain size with the flow stress (estimated in the range of 110-190 MPa with recrystallized grain size piezometry) during viscous deformation before and after the transient brittle event of stage (2).

During stage (2) the development of cataclasite and related dilatancy resulted in an increase of permeability and thus facilitated fluid access and fluid mobility in the shear zone. This enhanced mineral transformations as testified by modal enrichment of stilpnomelane (by biotite breakdown) and Na-amphibole in the ultramylonite.

Therefore, the observed structures witness a change in deformation style (from distributed to localized strain in brittle precursor), and a switch in the dominant deformation mechanism (from low T plasticity in the host rock to cataclasis and back to crystal plasticity in the ultramylonite), which occurred at the footwall of subduction interface at temperature conditions typical of the brittle/viscous transition in quartz/feldspathic rocks.

Finally, the transition from stage (2) and stage (3) is consistent with the general observation that nucleation of localized ductile shear zones requires the presence of a planar compositional or structural precursor (e.g. Pennacchioni and Zucchi, 2012, and references therein). The example from the Popolasca granite demonstrates that (i) nucleation on brittle precursors also occurs under HP/LT conditions in the subduction channel, and (ii) the brittle precursors are not necessarily inherited from an earlier deformation event, but can be the manifestation of switches in deformation mode in the footwall of the subduction interface.

7.2 Significance of the switch in deformation mode and implications for fault-slip behaviours in subduction zones

We interpreted the inferred deformation sequence and structures as the result of transient instabilities (Sibson, 1980; White, 1996; Handy and Brun, 2004) possibly representative of mixed fault-slip behaviours at seismogenic depth in the subduction channel. We have estimated the conditions resulting in the transient brittle event during stage (2) under the following assumptions and approximations:

1. The coefficient of internal friction, μ_i, is generally between 0.5 and 1.0 in intact rocks (Sibson, 1985). We considered $\mu_i = 0.6$ in the failure envelope for the intact Popolasca granitoid.
2. We used a cohesive strength of 35 MPa as representative for granitoids (Amitrano and Schmittbuhl, 2002), with a resulting tensile strength of 17.5 MPa.
3. We assumed and Andersonian stress field and a thrust regime. The effective vertical stress σ'_v corresponds to the effective minimum principal stress $\sigma'_3 = \sigma_3 - P_f$, where P_f is the pore fluid pressure. We considered a hydrostatic pore pressure ($\lambda = 0.4$, $P_f = 320$ MPa for $\sigma_3 = 800$ MPa) during the formation of the gneissic foliation in the host rock.
4. We assumed a differential stress of 110-190 MPa during viscous flow of the granitoid prior to

Solid Earth Discuss., doi:10.5194/se-2017-11, 2017
Manuscript under review for journal Solid Earth
Published: 7 February 2017

brittle failure at σ'_v = 480 MPa, as derived from the recrystallized grain size piezometry in the protomylonite.

The results of our analysis are shown in Fig. 9a. For brittle failure, it is necessary to invoke high differential stresses (of the order of 1.1 GPa assuming a hydrostatic pore fluid pressure), or higher fluid pressure (Fig. 9a). Differential stresses in excess of 1 GPa have been associated with intermediate depth (50-300 km) earthquakes in the subduction channel (e.g. John et al., 2009), and are expected to result in extensive development of pseudotachylytes in granitoid rocks (e.g. Austrheim 2013 and references therein), which, on the contrary, have not been observed in the sample studied here.

For the differential stress range and the vertical stress considered here, brittle failure requires (sub)lithostathic fluid pressure ($0.96 < \lambda < 1$, Fig. 9). The strength envelope plotted for pore fluid pressure between 0.98 and 0.94 and for a strain rate of 10^{-12} s^{-1} (Fig. 9b) suggests that viscous deformation at the estimated depth range (23-30 km) is only possible for pore fluid pressure ≤ 0.94, otherwise brittle deformation is expected to occur. Thus, under the assumptions listed above, our analysis indicates that local fluctuations in pore fluid pressure can explain the cyclic viscous-brittle-viscous deformation switch. However, despite the synkinematic growth of hydrous minerals in the cataclasite and the high pore fluid pressure required at failure, there is no evidence of macroscopic veining or hybrid fractures in the samples. Our analysis is consistent with this observation, in that failure occurs entirely in the shear fractures field and not in the (hybrid) shear extension fractures field (Fig. 9a).

Drawing from the results shown in Figs. 9a,b and using concept and inferences coming from modern studies of convergent subduction system (e.g. Ozowa et al., 2002; Fu and Freymuller, 2013; Bedford et al., 2013) we may suggest the following deformation path (Fig.10) for the structural features of our analysed sample. A first stage of distributed deformation (stage 1) may be associated with large scale anastomosed shear zone development and aseismic creep, then, following Angiboust et al. (2015), two possible deformation scenario and slip patterns may be envisaged: (a) propagation at seismic rate of microrupture followed by afterslip or (b) slow slip phenomena in an aseismically creeping crust. In the first case transient strain rate increase associated with brittle fracturing would represent the deep response of the transition zone to a specific stage of the seismic cycle taking place higher up along the seismogenic portion of the subduction interface (Fig.10c, scenario 1) or in less deformed domains acting as local stress raisers nearby (Fig.10c, scenario 2). Cataclastic deformation would then correlate with coseismic to postseismic deformation higher up along the interface. In that case, the mylonitization of the brittle precursor would be the record of subsequent interseismic deformation at lower strain rates, taking place in the time frame between two earthquakes.

In the second case (Fig.10d), the transient highs in strain rates related to brittle fracturing and cataclasis

Solid Earth Discuss., doi:10.5194/se-2017-11, 2017
Manuscript under review for journal Solid Earth
Published: 7 February 2017

could be the field evidence of deformation associated with slow slip events (SSEs) or other transient slips, generally localized along the subduction interface at this depth range itself (e.g., Shelly et al., 2006; Fagereng et al., 2014). We are aware that the mechanism(s) of SSEs initiation are still poorly understood, and that stress/strain rate perturbations triggered by an earthquake nearby followed by postseismic slip and interseismic creep is an equally feasible mechanism to explain the deformation sequence recorded in our sample. However, our preferred interpretation is that the transient brittle deformation recorded in our studied sample is the manifestation of a slow slip event, for the following reasons: (1) subduction interface SSEs typically occur at the downdip transition from stick-slip behaviour to aseismic creep (e.g. Wallace and Beavan, 2010), and, in granitoid rocks, this transition is expected to occur at the T range of deformation of our case-study, as witnessed by the deformation microstructures of quartz and feldspar in the host protomylonite; (2) SSEs are often related to high pore fluid pressure (e.g. Liu and Rice, 2007).

Whatever the actual process triggering brittle deformation was, we want to emphasize that detailed microstructural studies of exhumed shear zones are a valuable complement to the geodetic, seismological and experimental studies that aim to unravel the complex fault-slip behaviours at the subduction interface. In this context, our studied sample represents a new and still not yet documented case study of brittle-viscous transition zone and processes in subducted continental crust. Moreover, our study reinforces the concept that the external zones of Alpine Corsica represent a unique target to document and understand footwall deformation structures and processes related with HP/LT continental subduction.

8. References

Altenberger, U., Prosser, G., Grande, A., Günter, C., and Langone, A.: A seismogenic zone in the deep crust indicated by pseudotachylytes and ultramylonites in granulite-facies ricks of Calabria (Southern Italy), Contributions to Mineralogy and Petrology, 166, 975-994, 2013.

Amitrano, D., and Schmittbuhl, J.: Fracture roughness and gouge distribution of a granite shear band, Journal of Geophysical Research, 107, B12, doi:10.1029/2002JB001761, 2002.

Andersen, T.B., and Austrheim, H.: Fossil earthquakes recorded by pseudotachylytes in mantle peridotites from the Alpine subduction complex of Corsica. Earth and Planetary Science Letters 242, 58-72, 2006

Andersen, T.B., Austrheim, H., Deseta, N., Silkoset, P., and Ashwal, L.D.: Large subduction earthquakes along the fossil Moho in Alpine Corsica. Geology, 42, 395-398, 10.1130/G35345.1, 2014.

Angiboust, S., Glodny, J., Oncken, O., Chopin, C. In search of transient subduction interfaces in the Dent Blanche–Sesia Tectonic System (W. Alps), Lithos, 205, 298-321, 2014.

Angiboust, S., Kirsch, J., Oncken, O., Glodny, J., Monié, P., and Rybacki, E.: Probing the transition between seismically coupled and decoupled segments along an ancient subduction interface. Geochemistry Geophysics Geosystems, 16, 1905-1922, doi:10.1002/2015GC005776, 2015.

Atkinson, B.K.: Subcritical crack propagation in rocks: theory, experimental result and applications. Journal of Structural Geology, 4: 41–56, 1982.

Austrheim, H.: Fluid and deformation induced metamorphic processes around Moho beneath continent collision zones: Examples from the exposed root zone of the Caledonian mountain belt, W-Norway, Tectonophysics, 609, 620-635, 2013.

Austrheim, H. and Andersen T.B.: Pseudotachylytes from Corsica: fossil earthquakes from a subduction complex. Terra Nova, 16, 193-197, 2004.

Austrheim, H., and Boundy, T.M.: Pseudotachylytes generated during seismic faulting and eclogitization of the deep crust: Science, 265: 82-83, 1994.

Bedford, J., Moreno, M., Baez, J.C., Lange, D., Tilmann, F., Rosenau, M., Heibach, O., Oncken, O., Bartsch, M., Rietbrock, A., Tassara, A., Bevis, M., and Vigny, C.,: A high-resolution, time-variable afterslip model for the 2010 Maule Mw 8.8, Chile megathrust earthquake, Earth Planet. Sci. Lett., 383, 26–36, 2013.

Berger, A. and Bousquet, R.: Subduction-related metamorphism in the Alps: review of isotopic ages based on petrology and their geodynamic consequences. Geological Society, London, Special Publications, 298, 117-144, 2008.

Beroza, G.C. and Ide, S.: Slow Earthquakes and Non-volcanic Tremor, Annual Review of Earth and Planetary Sciences, 39, 271-296, 2011.

Bestmann, M, and Prior, D.J.: Intragranular dynamic recrystallization in naturally deformed calcite marble: diffusion accommodated grain boundary sliding as a result of subgrain rotation recrystallization, Journal of Structural Geology, 25, 1597-1613, 2003.

Bezert, P., Caby, R.: Sur l'age post-bartonien des événements tectono-métamorphiques alpines en bourdure orientale de la Corse cristalline. Bulletin de la Société Géologique de France, 8, 965–971, 1988.

Bos, B., Spiers, C.J.: Frictional-viscous flow of phyllosilicate-bearung rocks: Microphysical model and implications for crustal strength profiles. Journal of Geophysical Research, 107, doi: 10.1029/2001JB000301, 2002.

Burg, J.P, Laurent, P.: Strain analysis of a shear zone in a granodiorite. Tectonophysics 47:15-42. doi:10.1016/0040-1951 (78)90149-X, 1978.

Butler, R.H.W.: Area balancing as a test of models for the deep structure of mountain belts, with specific reference to the Alps. Journal of Structural Geology 52, 2-16, 2013.

Carminati, E., and Doglioni, C.: Alps vs. Apennines: The paradigm of a tectonically asymmetric Earth, Earth-Science Reviews 112 67–96: 2012.

Chester, F.M.: Dynamic recrystallization in semi-brittle faults. Journal of Structural Geology 11, 847-858, 1989.

Cooper, F. J., Platt, J. P., Platzman, E. S., Grove, M. J., and Seward, G.: Opposing shear senses in a subdetachment mylonite zone: Implications for core complex mechanics. Tectonics, 29, 10.1029/2009TC002632, 2010.

Derez, T., Pennock, G., Drury, M., and Sintubin, M.: Low-temperature intracrystalline deformation microstructures in quartz. Journal of Structural Geology, 71, 3-23, 2015.

Deseta, N., Andersen, T.B., and Ashwal, L.D.: A weakening mechanism for intermediate depth seismicity? Detailed petrographic and microstructural observation from blueschist facies pseudotachylytes, Cape Corse, Corsica. Tectonophysics 610, 138-149, 2014a

Deseta, N., Ashwal, L.D., and Andersen, T.B.: Initiating intermediate-depth earthquakes: Insights from a HP-LT ophiolite from Corsica. Lithos, 206, 127-146, 2014b.

Di Rosa, M., De Giorgi, A., Marroni, M. and Vidal., O. Syn-convergent exhumation of continental crust: evidence from structural and metamorphic analysis of the Monte Cecu area, Alpine Corsica (Northern Corsica, France). Geological Journal, doi: 10.1002/gj.2857: 2016.

Di Vincenzo, G., Grande, A., Prosser, G., Cavazza, W., and De Celles, P.G.: 40Ar–39Ar laser dating of ductile shear zones from central Corsica (France): evidence of Alpine (middle to late Eocene) syn-burial shearing in Variscan granitoids, Lithos, doi: 10.1016/j.lithos.2016.07.022, 2016.

Evans, B.W.: Phase relations of epidote-blueschists. Lithos 25, 3–23, 1990.

Faccenna, C., Piromallo, C., Crespo-Blanc, A., Jolivet, L., and Rossetti, F.: Lateral slab deformation and the origin of the western Mediterranean arcs. Tectonics 23, TC1012, 2004.

Fagereng, Å, Hillary, G.W.B., and Diener, J.F.A.: Brittle-viscous deformation, slow slip, and tremor, Geophysical Research Letters, 41, 4159–4167, doi:10.1002/2014GL060433, 2014.

Fitz Gerald, J.D., and Stunitz, H.: Deformation of granitoids at low metamorphic grades. I. Reactions and grain size reduction. Tectonophysics 221, 269–297, 1993.

Fu, Y., and Freymueller, J.T.: Repeated large slow slip events at the south central Alaska subduction zone, Earth Planet. Sci. Lett., 375, 303–311, 2013.

Fusseis, F., and Handy, M.R.: Micromechanisms of shear zone propagation at the brittle–viscous transition. Journal of Structural Geology 30, 1242–1253, 2008.

Gapais, D., Bale, P., Choukroune, P., Cobbold, P.R., Mahjoub, Y., and Marquer, D.: Bulk kinematics from shear zone patterns: some field examples, Journal of Structural Geology, 9: 635-646. doi:10.1016/0191-8141(87) 90148-9, 1987.

Garfagnoli, F., Menna, F., Pandeli, E., and Principi, G.: Alpine metamorphic and tectonic evolution of the Inzecca-Ghisoni area (southern Alpine Corsica, France). Geological Journal, 44, 191–210, 2009.

Gibbons, W., and Horak, J.: Alpine metamorphism of Hercynian hornblende granodiorite beneath the blueschist facies schistes lustre´s nappe of NE Corsica. Journal of Metamorphic Geology 2, 95-113, 1984.

Golcalves, P-. Poilvet, J-C., Oliot, E., Trap, P., Marquer, D.: How does shear zone nucleate? An example from the Suretta nappe (Swiss Eastern Alps). Journal of Structural Geology 86, 166-180, 2016.

Guermani, A., and Pennacchioni, G: Brittle precursors of plastic deformation in a granite: An example from the Mont Blanc Massif (Helvetic, western Alps), Journal of Structural Geology, 20, 135–148, 1998.

Gueydan, F., Brun, J.P., Philippon, M., and Noury, M.: Sequential extension as record of Corsica rotation during Apennines slab roll-back. Tectonophysics, doi: 10.1016/j.tecto.2016.12.028, 2016.

Hacker, B.R., Peacock, S.M., Abers, G.A., Holloway S.D. Subduction factory 2. Are intermediate - depth earthquakes in subducting slabs linked to metamorphic dehydration reactions? Journal of Geophysical Research, 108, doi:10.1029/2001JB001129, 2003.

Handy, M.R., and Stunitz, H.: Strain localization by fracturing and reaction-weakening - a mechanism for initiating exhumation of subcontinental mantle beneath rifted margins. In: De Meer S., Drury M.R., De Bresser J.H.P., Pennock GM (eds) Deformation mechanisms, rheology and tectonics: current status and future perspectives, 200. Geological Society of London Special Publication, 387–407, 2002.

Handy M.R., and Brun, J.P.: Seismicity, structure and strength of the continental lithosphere. Earth and Planetary Science Letters 223, 427– 441, 2004.

Handy M.R., Hirth, G., and Burgmann, R.: Continental fault structure and rheology from frictional-to-viscous transition downward. In Tectonic Faults: Agents of Change on a Dynamic Earth. Handy, M.R., Hirth, G. and Hovious, N eds. Dahlem Workshop Reports, MIT press, 139-181, 2007.

Hayman, N.W., and Lavier, L.L.: The geologic record of deep episodic tremor and slip, Geology, 42, 195–198, doi:10.1130/G34990.1, 2014.

Healy, D., Reddy, S.M., Timms, N.E., Gray, E.M., and Vitale Brovarone, A.: Trench parallel fast axes of seismic anisotropy due to fluid-filled cracks in subducting slabs. Earth and Planetary Science Letters 283, 75-86, 2009.

Hirth, G., and Tullis, J.: Dislocation creep regimes in quartz aggregates, Journal of Structural Geology, 14: 145–159, 1992

Hirth, G., Teyssier, C., and Dunlop, W.J.: An evaluation of quartzite flow laws based on comparisons between experimentally and naturally deformed rocks, International Journal of Earth Sciences, 90, 77-87, 2001.

John, T., Medvedev, S., Rüpke, L.H., Andersen, T.B., Podladchikov, Y.Y., and Austrheim, Å.: Generation of intermediate-depth earthquakes by self-localizing thermal runaway, Nature Geoscience, 2, 137-140, doi:10.1038/NGEO419, 2009.

Jolivet, L., Dubois, R., Fournier, M., Goffé, B., Michard, A., Jourdan, C.: Ductile extension in Alpine Corsica. Geology 18, 1007-1010, 1990.

Kjøll, H.J., Viola, G., Menegon, L., and Sørensen, B.E.: Brittle-viscous deformation of vein quartz under fluid-rich lower greenschist facies conditions. Solid Earth, 6, 681-699, 2015.

Kohlstedt, D.L., Evans, B., and Mackwell, S.J.: Strength of the lithosphere: Constraints imposed by laboratory experiments, Journal of Geophysical Research, 100, 17857-17602, 1995.

Kruhl, J.H.: Prism- and basal-plane parallel subgrain boundaries in quartz: a microstructural geothermobarometer, Journal of Metamorphic Geology, 14, 581-589, 1996.

Küster, M, and Stöckhert, B.: High differential stress and sublithostatic pore fluid pressure in the ductile regime — microstructural evidence for short-term post-seismic creep in the Sesia Zone, Western Alps, Tectonophysics, 303, 263-277, 1999.

Lamb, S.: Shear stresses on megathrusts: Implications for mountain building behind subduction zones, J. Geophys. Res., 111, B07401, doi:10.1029/2005JB003916, 2006.

Liu, Y., and Rice, J.R.: Spontaneous and triggered aseismic deformation transients in a subduction fault model, J. Geophys. Res., 112, B09404, doi:10.1029/2007JB004930, 2007.

Maggi, M., Rossetti, F., Corfu, F., Theye, T., Andersen, T.B.: Faccenna, C., Clinopyroxene-rutile phyllonites from the East Tenda Shear Zone (Alpine Corsica, France): pressure-temperature-time constraints to the Alpine reworking of Variscan Corsica. Journal of the Geological Society 169, 723-732, 2012.

Magott, R., Fabbri, O., Fournier, M.: Subduction zone intermediate-depth seismicity: Insights from the structural analysis of Alpine high-pressure ophiolite-hosted pseudotachylytes (Corsica, France). Journal of Structural Geology 87, 95-114, 2016.

Magott, R., Fabbri, O., Fournier, M.: Polyphase ductile/brittle deformation along a major tectonic boundary in an ophiolitic nappe, Alpine Corsica: Insights on subduction zone intermediate-depth asperities Journal of Structural Geology 87, 95-114, 2016.

Malatesta, C., Federico, L., Crispini, L., Capponi, G.,: Fluid-controlled deformation in blueschist-facies conditions: plastic vs brittle behaviour in a brecciated mylonite (Voltri Massif, Western Alps, Italy) Geological Magazine, doi:10.1017/S0016756816001163, 2017.

Malasoma, A., Marroni, M., Musumeci, G., Pandolfi, L.: High pressure mineral assemblage in granitic rocks from continental units in Alpine Corsica, France. Geological Journal, 41, 49–59, 2006

Mancktelow, N.S.: How ductile are ductile shear zones? Geology, 34, 345-348, 2006

Mancktelow, N.S., and Pennacchioni, G.: The control of precursor brittle fracture and fluidrock interaction on the development of single and paired ductile shear zones. Journal of Structural Geology, 4, 27, 645–661, 2005.

Massonne, H.J., and Szpurka, Z.: Thermodynamic properties of white micas on the basis of high-pressure experiments in the systems K2OMgO-Al2O3-SiO2-H2O and K2O-FeO-Al2O3-SiO2-H2O. Lithos 41, 229-250, 1997.

Mattauer, M., Faure, M. and Malavieille, J.: Transverse lineation and large scale structures related to Alpine obduction in Corsica. Journal of Structural Geology, 3, 401- 409, 1981.

Mazzoli, S., Vitale, S., Del Monaco, G., Guerriero, G., Margottini, C., and Spizzichino, D.: 'Diffuse faulting' in the Machu Pichu granitoid pluton, Eastern Cordillera, Perù. Journal of Structural Geology, 31, 1395- 1408, 2009.

Meneghini, F., Di Toro, G., Rowe, C. D., Moore, J. C., Tsutsumi, A., and Yamaguchi, A.: Record of mega-earthquakes in subduction thrusts: The black fault rocks of Pasagshak Point (Kodiak Island, Alaska), Geol. Soc. Am. Bull., 122(7–8), 1280–1297, 2010.

Menegon, L., and Pennacchioni, G.: Local shear zone pattern and bulk deformation in the Gran Paradiso metagranite (NW Italian Alps), International Journal of Earth Sciences, 99, 1805-1825, 2010.

Menegon, L., Piazolo, S. and Pennacchioni, G.: The effect of Dauphiné twinning on plastic strain in quartz, Contributions to Mineralogy and Petrology, 161, 635-652, 2011.

Menegon, L., Stünitz, H., Nasipuri, P., Heilbronner, R., and Svahnberg, H.: Transition from fracturing to viscous ow in granulite facies perthitic feldspar (Lofoten, Norway), Journal of Structural Geology, 48, 95-112, 2013.

Molli, G., Malavieille, J.: Orogenic processes and the Alps/Apennines geodynamic evolution: insights from Taiwan. Int J Earth Sci, 100: 1207-1224, doi: 10.1007/s00531-010-0598-y, 2011.

Molli., G., Malasoma, A., Meneghini, F.: Brittle precursors of HP/LT microscale shear zone: a case study from Alpine Corsica. 15th Conference of Deformation, Rheology and Tectonics, Zurich, Abstract Volume, 153, 2005.

Molli, G.: Localizzazione di zone di taglio HP/LT su precursori fragili: Un esempio dalla Corsica Alpina, Rend. Soc. Geol. It., 4 Nuova Serie, 270-271, 2007.

Molli, G.: Northern Apennine-Corsica orogenic system: an updated review. In: Siegesmund, S., Fugenschuh, B., Froitzheim, N. (Eds.), Tectonic Aspects of the Alpine-Dinaride-Carpathian System.

Geological Society, London Special Publications, 298, 413- 442, 2008.

Molli, G., White, J.C., Kennedy, L., and Taini, V.: Low-temperature deformation of limestone, Isola Palmaria, Northern Apennine, Italy - The role of primary textures, precursory veins and intracrystalline deformation in localization. Journal of Structural Geology, 33, 255-270, doi: 10 .1016 /j .jsg .2010 .11 .015, 2011.

Neumann, B.: Texture development of recrystallised quartz polycrystals unravelled by orientation and misorientation characteristics. Journal of Structural Geology, 22, 1695-1711, 2000.

Ozawa, S., Murakami, M., Kaidzu, M., Tada, T., Sagiya, T., Hatanaka, Y., Yarai, H., and Nishimura, T.: Detection and monitoring of ongoing aseismic slip in the Tokai region, central Japan, Science, 298(5595), 1009–1012, 2002.

Passchier, C.W., and Trouw, R.A.J.: Microtectonics. Springer. 366p., 2011.

Pec, M, Stünitz, and Heilbronner, R.: Semi-brittle deformation of granitoid gouges in shear experiments at elevated pressures and temperatures, Journal of Structural Geology, 38, 200-221, 2012.

Peng, Z., and Gomberg, J.: An integrated perspective of the continuum between earthquakes and slow slip phenomena, Nature Geoscience, 3, 599–607, 2010.

Pennacchioni, G.: Control of the geometry of precursor brittle structures on the type of ductile shear zone in the Adamello tonalites, Southern Alps (Italy), Journal of Structural Geology, 27, 627-644, 2005

Pennacchioni, G., and Mancktelow, N.S.: Nucleation and initial growth of a shear zone network within compositionally and structurally heterogeneous granitoids under amphibolite facies conditions, Journal of Structural Geology, 29, 1757-1780, 2007.

Pennacchioni, G., and Zucchi, E.: High temperature fracturing and ductile deformation during cooling of a pluton: The Lake Edison granodiorite (Sierra Nevada batholith, California), Journal of Structural Geology, 50, 54-81, 2013.

Pennacchioni, G., Di Toro, G., Brack, P., Menegon, L., and Villa, I.M.: Brittle–ductile–brittle deformation during cooling of tonalite (Adamello, Southern Italian Alps), Tectonophysics 427, 171–197, 2006.

Pittarello, L., Pennacchioni, G., and Di Toro, G.: Amphibolite-facies pseudotachylytes in Premosello metagabbro and felsic mylonites (Ivrea Zone, Italy), Tectonophysics, 580, 43-57, 2012.

Platt, J.P., and Behr, W.M.: Lithospheric shear zones as constant stress experiments, Geology, 39, 127-130, doi: 10.1130/G31561.1, 2011.

Polino, R., Dal Piaz, G.V., and Gosso, G.: Tectonic erosion at the Adria margin and accretionary process for the Cretaceous orogeny of the Alps. In: Roure, F., Heitzman, P., and Polino, R. (eds) Deep Structure of the Alps. Volume Speciale Società Geologica Italiana, Roma, 1, 345–367, 1990.

Prior, D.J., Wheeler, J., Peruzzo, L., Spiess, R., and Storey, G.: Some garnet microstructures: an illustration of the potential of orientation maps and misorientation analysis in microstructural studies. Journal of Structural Geology, 24, 999-1011, 2002.

Ramsay, J.G., and Graham, R.H.: Strain variation in shear belts. Canadian Journal Earth Science 7, 786–813, 1970.

Rosenberg, C., and Kissling, E.: Three-dimensional insight into Central-Alpine collision: Lower-plate or upper-plate indentation? Geology, 41, 1219-1222, doi:10.1130/G34584.1, 2013.

Rossi, P., Durand-Delga, M., Lahondére, J. C., and Lahondére, D.: Carte géologique de la France à 1/50.000, feuille Santo Pietro di Tenda, BRGM, 2003.

Rutter, E. H: On the nomenclature of mode of failure transitions in rocks, Tectonophysics, 122 (3-4), 381- 387. 1986.

Schiffman, P., and Day, H.W.: Petrologic methods for the study of Very Low-grade metabasites in Low-Grade metamorphism (eds M. Frey and D. Robinson), Blackwell Publishing Ltd., Oxford, UK: doi: 10.1002/9781444313345.ch4, 2009.

Schmid, S.M., and Handy, M.R.: Towards a genetic classification of fault rocks: Geological usage and tectonophysical implications, in Muller, D.W., et al., eds., Controversies in modern geology: London, Academic Press, 339–361. 1991.

Schmid, S. M., Pfiffer, O.A., Froitzheim, N., Schonborn, G. and Kissling, E., Geophysical-geological transect and tectonic evolution of the Swiss-Italian Alps. Tectonics, 12, 1036-1064: 1996.

Scholz, C.H.: The brittle-plastic transition and the depth of seismic faulting. Geologische Rundschau, 77, 319-328, 1988.

Scholz, C.H.: The Mechanics of Earthquakes and Faulting, 2nd ed., Cambridge University Press, 2002.

Segall, P., and Simpson, C.: Nucleation of ductile shear zones on dilatant fractures, Geology, 14, 56–59, 1986.

Shimamoto, T.: The origin of S-C mylonites and a new fault-zone model, Journal of Structural Geology 11, 51-64, 1989.

Shimamoto, T., Logan, J.M. Velocity-dependent behaviours of simulated halite shear zones: an analog for silicates. Am. Geophys. Mongr., 37, 49-63, 1986.

Sibson, R.H.: Fault rocks and fault mechanisms, Journal of the Geological Society of London, 133, 191-213, 1977.

Sibson, R.H: Transient discontinuities in ductile shear zones, Journal of Structural Geology, 2, 165–171, 1980.

Sibson, R.H.: Continental fault structure and the shallow earthquake source, Journal of the Geological Society of London, 140, 741-767, 1983.

Sibson, R.H.: A note on fault reactivation, Journal of Structural Geology 7, 751–754, 1985.

Simpson, C.: Deformation of granitic rocks across the brittle-ductile transition, Journal of Structural Geology 7: 503-511, 1985.

Simpson, C.: Fabric development in brittle-to-ductile shear zones, Pure and Applied Geophysics 124 (1-2), 269–288, 1986.

Stipp, M., Stunitz, H., Heilbronner, R. and Schmid, S.M.: The eastern Tonale fault zone: a 'natural laboratory' for crystal plastic deformation of quartz over a temperature range from 250 to 700 °C. J Struct Geol, 24, 1861-1884, 2002.

Stipp, M., and Tullis, J.: The recrystallized grain size piezometer for quartz, Geophysical Research Letters, 30, 21, 2088, doi:10.1029/2003GL018444, 2003.

Stöckhert, B.: Stress and deformation in subduction zones - insight from the record of exhumed metamorphic rocks, in Geological Society of London Special Publication, S. de Meer, et al., Editors.: London, 255-274, 2002.

Takagi, H., Goto, K., Shigematsu, N. Ultramylonite bands derived from cataclasite and pseudotachylyte in granites, northeast Japan., J Struct Geol, 22, 1325-1339, 2000.

Tödheide, K.: Water at high temperatures and pressures, in Water: A Comprehensive Treatise, vol. 1, edited by F. Franks, chap. 13, pp. 463–514, Springer, New York, 1972.

Trepmann, C.A., Stockhert, B., Dorner, D., Moghadam, E.H., Kuster, M. and Roller, K.: Simulating coseismic deformation of quartz in the middle crust and fabric evolution during postseismic stress relaxation – an experimental study. Tectonophysics 442, 83–104, 2007.

Tribuzio, R., and Giacomini, F., Blueschist facies metamorphism of peralkaline rhyolites from the Tenda crystalline massif (northern Corsica): evidence for involvement in the Alpine subduction event? Journal of Metamorphic Geology 20, 513-526, 2002.

Van Daalen, M., Heilbronner, R., Kunze, K.: Orientation analysis of localized shear deformation in quartz fibres at the brittle–ductile transition, Tectonophysics, 303, 83-107, 1999.

Vannucchi, P., Remitti, F., and Bettelli, G.: Geological record of fluid flow and seismogenesis along an erosive subducting plate boundary, Nature. 451, 7179,699-703, 2008.

Vernooij, M. G., den Brok, B., and Kunze, K.: Development of crystallographic preferred orientations by nucleation and growth of new grains in experimentally deformed quartz single crystals, Tectonophysics, 427, 35–53, 2006a.

Vernooij, M.G.C., Kunze, K. and den Brok, B.: 'Brittle' shear zones in experimentally deformed quartz single crystals. J Struct Geol 28: 1292–1306, 2006b

Viola, G., Mancktelow, N. S., and Miller, J. A.: Cyclic frictional– viscous slip oscillations along the base of an advancing nappe complex: insights into brittle-ductile nappe emplacement mechanisms from the Naukluft Nappe Complex, central Namibia, Tectonics, 25, TC3016, doi:10.1029/2005 tc 001939, 2006.

Vitale Brovarone, A., Beyssac, Ol., Malavieille, J., Molli, G., Beltrando, M., and Compagnoni, R. Stacking and metamorphism of continuous segments of subducted lithosphere in a high-pressure wedge:

The example of Alpine Corsica (France). Earth-Science Reviews, 116, 35–56, 2013.

Wallace, L.M. and Beavan, J.: Diverse slow slip behavior at the Hikurangi subduction margin, New Zealand, Journal of Geophysical Research, 115, B12402, doi:10.1029/2010JB007717, 2010.

White, J.C. and White, S.H.: Semi-brittle deformation within the Alpine fault zone, New Zealand. J Struct Geol 5: 579-589, 1982

White, J.C.: Transient discontinuities revisited: Pseudotachylyte, plastic instability and the influence of low pore fluid pressure on deformation processes in the mid-crust. J Struct Geol 18: 1471-1477, 1996.

Zibra, I., Kruhl, J.H., and Braga, R.: Late Palaeozoic deformation of post-Variscan lower crust: shear zone widening due to strain localization during retrograde shearing, International Journal of Earth Sciences, 99, 973-991, 2010.

Solid Earth Discuss., doi:10.5194/se-2017-11, 2017
Manuscript under review for journal Solid Earth
Published: 7 February 2017

Figures list and caption

Fig.1 a) Alpine Corsica within the Alps/Apennine framework. b) Tectonic map of north Corsica showing the main tectonic units and the area of studied sample. 1,2) Corsican continental crust, mainly Carboniferous-Permian granitoids, their host pre-Carboniferous basement and a Mesozoic to Eocene cover: (1a) "authochtonous" Hercynian Corsica and (1b) greenschist/lower-blueschist external continental units (Corte; Popolasca); 2) inner continental units: (2a) upper-blueschist units (Tenda Massif; Centuri) and (2b) eclogite slices (Serra di Pigno-Farinole); 3) Schistes Lustres nappe (undifferentiated); 4) Nappe Superiore i.e. upper non-metamorphic units (Balagne, Nebbio and Macinaggio units); 6) Miocene sediments; c) Regional cross-section with indication of study sample from Popolasca area.

Fig.2. Mesoscopic view of the analyzed sample: protomylonitic metagranite host with millimetre-scale ultramylonite localized after brittle precursor. All observable deformation structures were developed under HP/LT metamorphic conditions.

Fig.3. Microscopic views of host-rock showing Quartz microstructures typical of low temperature plasticity: a) intracrystalline deformation (undulatory extinction, deformation lamellae, deformation bands, localized extinction bands, LEBs) associated with recrystallization along intragranular conjugate shear bands sets; b) brittle fracturing in domino-style of K-feldspar associated with K-feldspar breakdown to albite, stilpnomelane and phengite; c) quartz deformation lamellae and intergranular recrystallization by bulging; d) K-feldspar intergranular recrystallization and albite-neocrystallization, recrystallization also observable along later cracks and microfractures (horizontal to sub-horizontal).

Fig.4 a) BSE image of the metamorphic mineral assemblage in the host granitoids of the studied sample; Ab, albite; Amp, Na-amphibole; Kfs, K-feldspar; Phe, phengite; Qtz, quartz; b) composition of sodic amphiboles, using the classification of Leake et al. (1997); c) estimated peak-metamorphic pressure/temperature conditions for the studied sample (cross-hatched area) constrained by the reactions indicated.

Fig.5 a) Microscopic view of millimetre-scale shear zone nucleated after brittle precursor, with indication of the structural-compositional domains within the shear zone. Domain 1 relict domain of cataclasite; Domain 2 phyllonite; Domain 3 ultramylonite; b) detail of the sharp shear-zone boundary heritage of former host-fracture contact and ultramylonite to phyllonite transition within the microscale shear zone are well observable; c) detail of domain 1, relict domain of cataclasite, mainly K-feldspar dominated. Angular fragments of variable size are indicative of brittle comminution.

Fig. 6 Microscopic view of ultramylonite; a) synkinematic Na-amphibole, boudinaged within the quartz and albite ultramylonite matrix; b) Quartz and albite recrystallized matrix, in the lower part the boundary of microscale shear zone with an host quartz porphyroclast; c) Quartz-ribbon with a strong elongation (1:15, X/Z ratio) defining a shape preferred orientation oblique (15°) to the shear zone boundary; d) detail of quartz recrystallization in the ribbon porphyroclast and matrix.

Fig. 7. EBSD analysis of quartz in the host protomylonite. (a) Microstructure of the analysed site. The white arrows indicate localized extinction bands that have been analysed with the boundary trace analysis and misorientation profiles as shown in Figs. 7b-g. (b) Inverse Pole Figure Map with the respect to the protomylonitic foliation in the host rock (vertical in the figure). Location of subset 1 and 2 and trace of misorientation profiles 1-3 are shown. (c) Pole figure of the host grain, colour coded per the quartz inverse pole figure shown in (b). (d) Pole figure of recrystallized quartz in the intracrystalline bands. The blue and red line indicates the average orientation of the trace of the intracrystalline bands with a subset 1 and 2 orientation, respectively. (e) Boundary trace analysis of the localized extinction band of subset 1. (f) Boundary trace analysis of the localized extinction band of subset 2. (g) Point-to-point misorientation profiles. See (b) for location of the traces of the profiles. (h) Misorientation axis of the host grain and of the recrystallized grains in sample coordinates.

Fig. 8. EBSD analysis of quartz in the ultramylonite. (a) Microstructure of the recrystallized quartz from domain 3 in the ultramylonite. (b) Pole figure of recrystallized quartz grains from (a). Only grains from recrystallized ribbons in the ultramylonite were analysed.

Fig.9. a) Brittle failure analysis for our studied sample, see text for assumptions and approximations. For the differential stress range and the vertical stress considered, brittle failure requires (sub)lithostathic fluid pressure ($0.96 < \lambda < 1$) whereas viscous deformation at the estimated depth range (23-30 km) is only possible for pore fluid pressure ≤ 0.94; b) Rheological profile calculated for a fixed strain rate of 10^{-12} s^{-2} (see text for calculation details) using the quartz flow law of Hirth et al. (2001). Cycle of switching in deformation style and mechanisms is suggested for the anayzed sample in its ambient depth-range. Frictional Byerlee envelope is calculated using an average friction coefficient of 0.7 for various pore fluid pressure ratio values (Fig.9a and text). Stress estimates based on recrystallized quartz piezometry (grey shaded area) have been calculated following Stipp and Tullis, (2003).

Solid Earth Discuss., doi:10.5194/se-2017-11, 2017
Manuscript under review for journal Solid Earth
Published: 7 February 2017

Fig.10. a) Simplified view of the ancient subduction of the corsican continental crust, with indication where the mechanical coupling is the highest (seismogenic zone) and lowest (stable slip). The white rectangle corresponds to the inferred zone of the studied sample. The pink to red shading figured the lower to higher blueschist- to eclogite-facies peak metamorphism in continental-derived crustal units; b,c,d Multi-stage scenario for development of the association of granitic protomylonites and ultramylonites from brittle precursors in the Popolasca area: a) General sketch showing the east-dipping ancient alpine subduction of the corsican continental crust. b): Formation of crustal scale anastomosed network of shear zones within the host granitic crust, active distributed deformation with aseismic creep; c: Formation of brittle instabilities (stage 2) in the shear zone by seismic ruptures nucleated along the subduction interface (1) or the core of granites (2) and having propagated across and beyond the granitic mylonites, followed by post-seismic creep, with locatization of shear zone after brittle precursor (stage 3); d) Formation of brittle instabilities by seismic tremors and slow-slip events followed by post-seismic (post-tremors) creep.

Solid Earth Discuss., doi:10.5194/se-2017-11, 2017
Manuscript under review for journal Solid Earth
Published: 7 February 2017

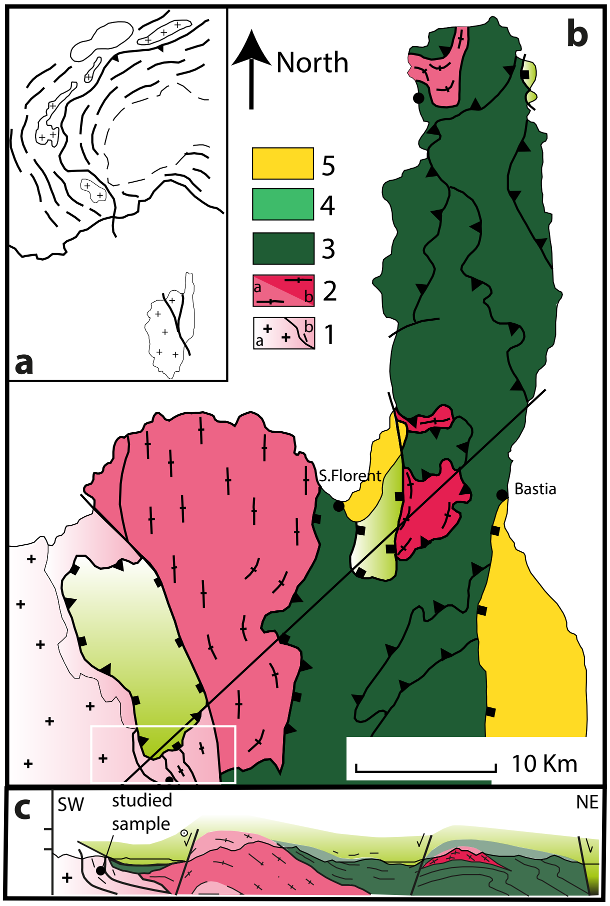

Fig.01

Solid Earth Discuss., doi:10.5194/se-2017-11, 2017
Manuscript under review for journal Solid Earth
Published: 7 February 2017

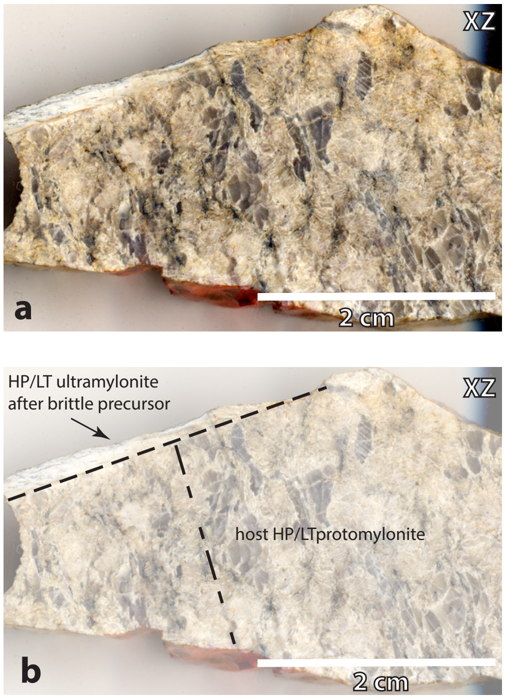

Fig.02

Solid Earth Discuss., doi:10.5194/se-2017-11, 2017
Manuscript under review for journal Solid Earth
Published: 7 February 2017

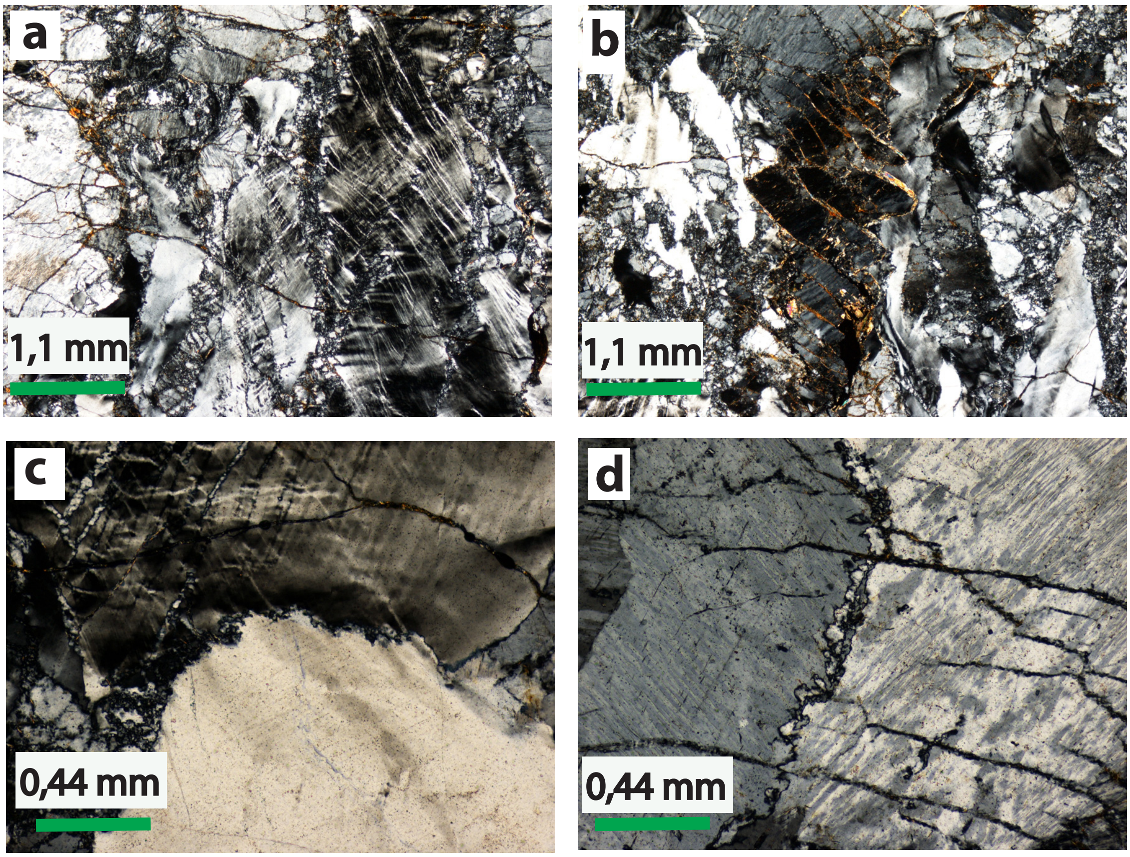

Fig.03

Solid Earth Discuss., doi:10.5194/se-2017-11, 2017
Manuscript under review for journal Solid Earth
Published: 7 February 2017

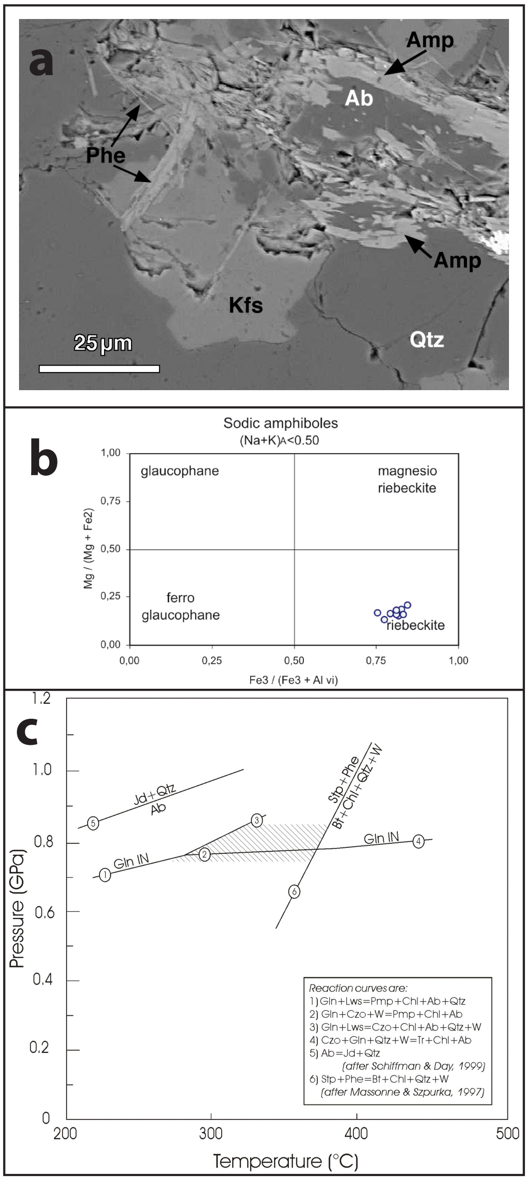

Fig.04

Solid Earth Discuss., doi:10.5194/se-2017-11, 2017
Manuscript under review for journal Solid Earth
Published: 7 February 2017

Solid Earth
Discussions
Open Access

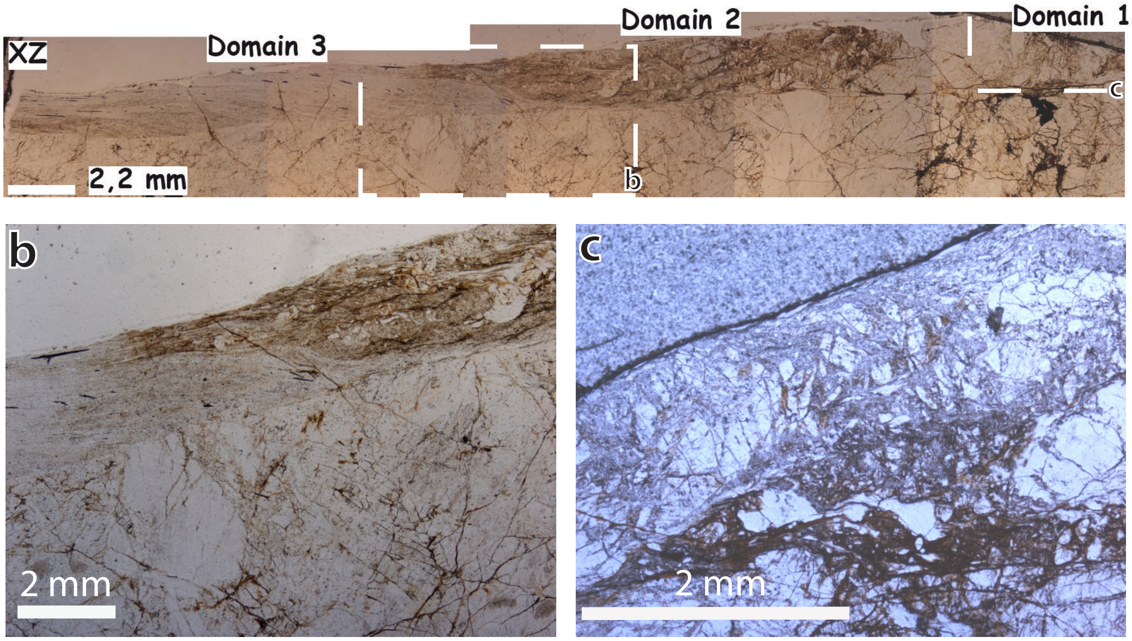

Fig.05

Solid Earth Discuss., doi:10.5194/se-2017-11, 2017
Manuscript under review for journal Solid Earth
Published: 7 February 2017

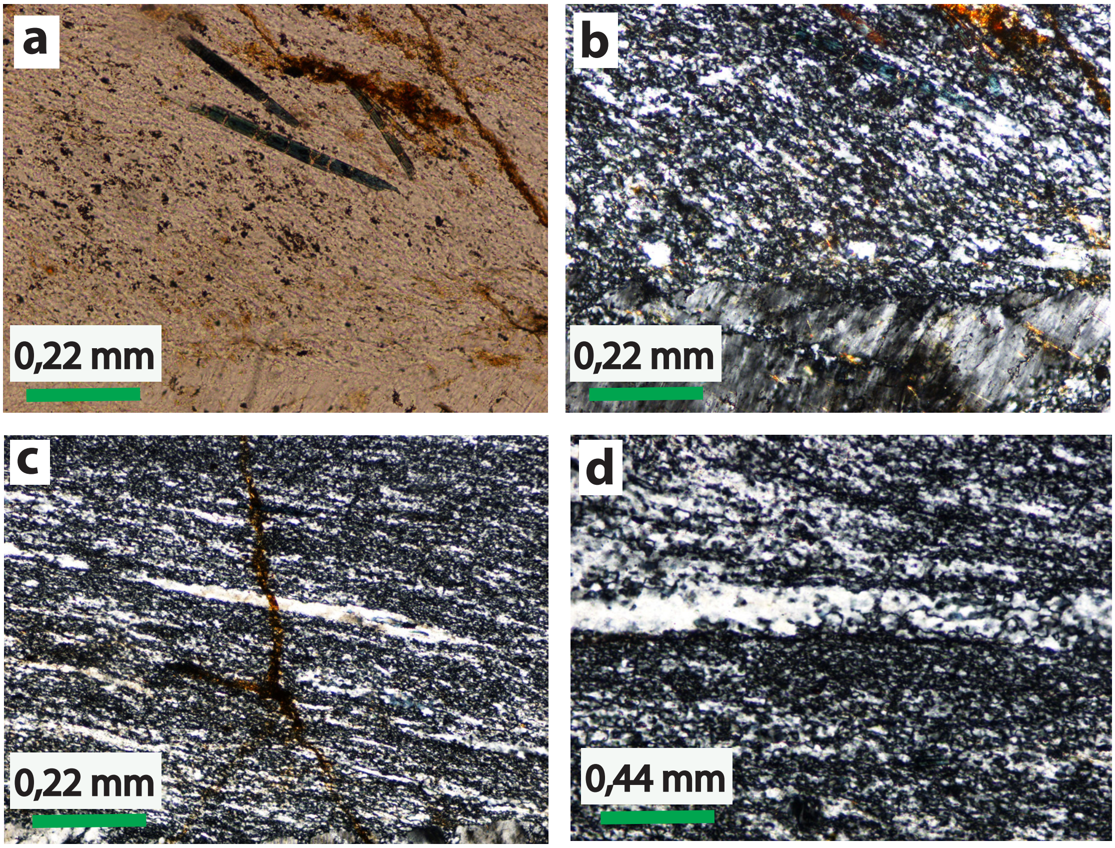

Fig.06

Solid Earth Discuss., doi:10.5194/se-2017-11, 2017
Manuscript under review for journal Solid Earth
Published: 7 February 2017

Fig.07

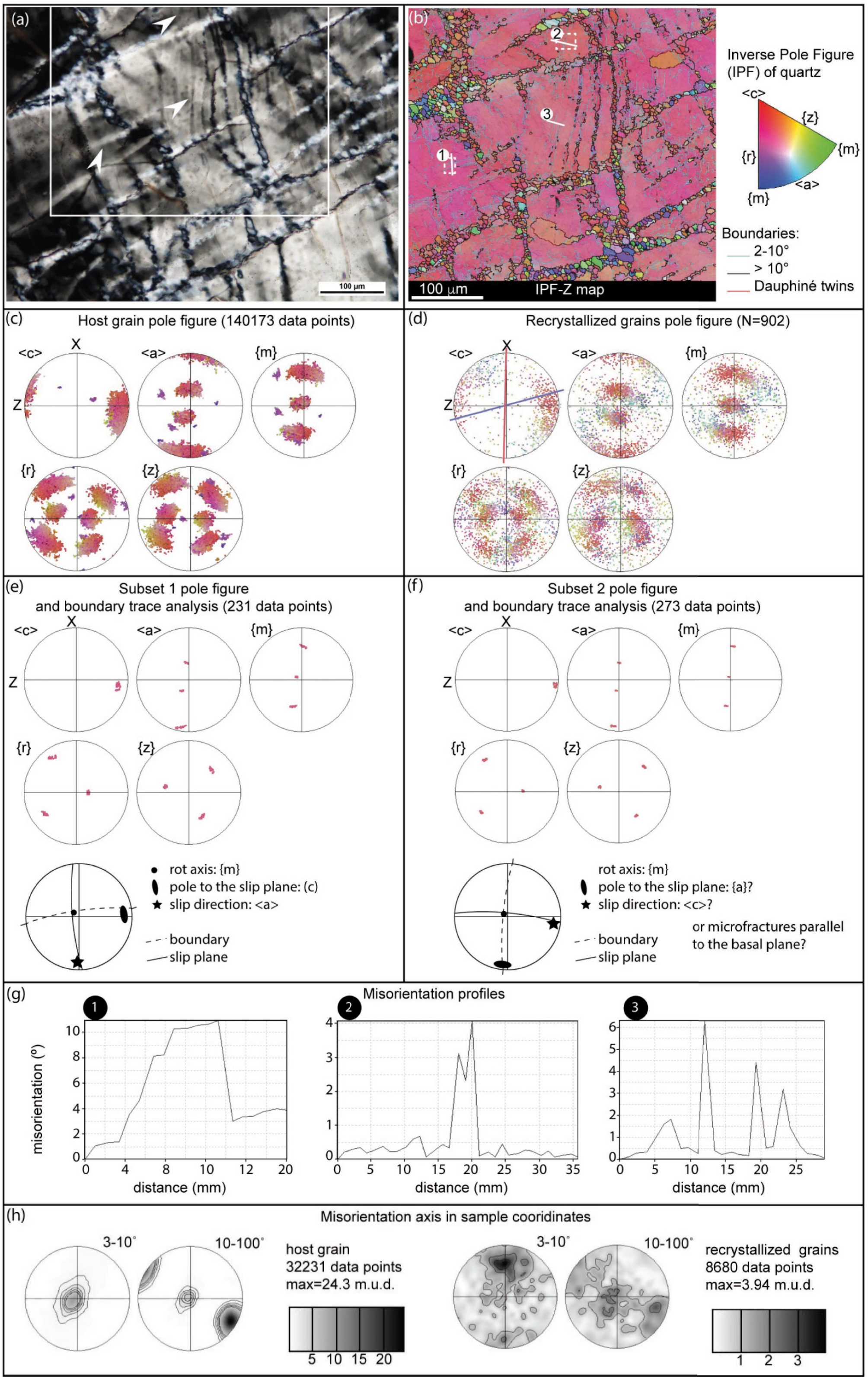

Solid Earth Discuss., doi:10.5194/se-2017-11, 2017
Manuscript under review for journal Solid Earth
Published: 7 February 2017

Solid Earth
Discussions
Open Access
EGU

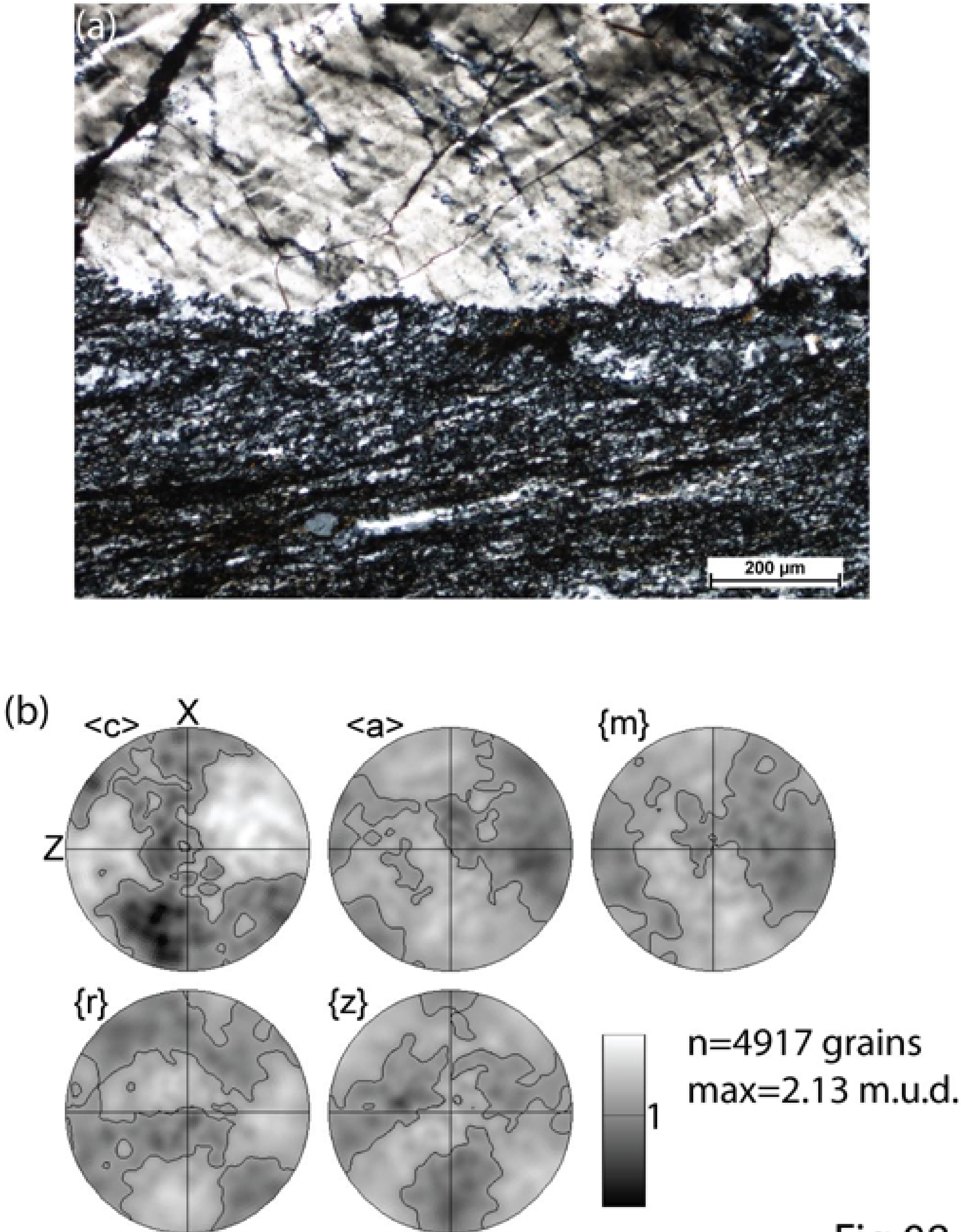

Fig.08

Solid Earth Discuss., doi:10.5194/se-2017-11, 2017
Manuscript under review for journal Solid Earth
Published: 7 February 2017

Solid Earth
Discussions

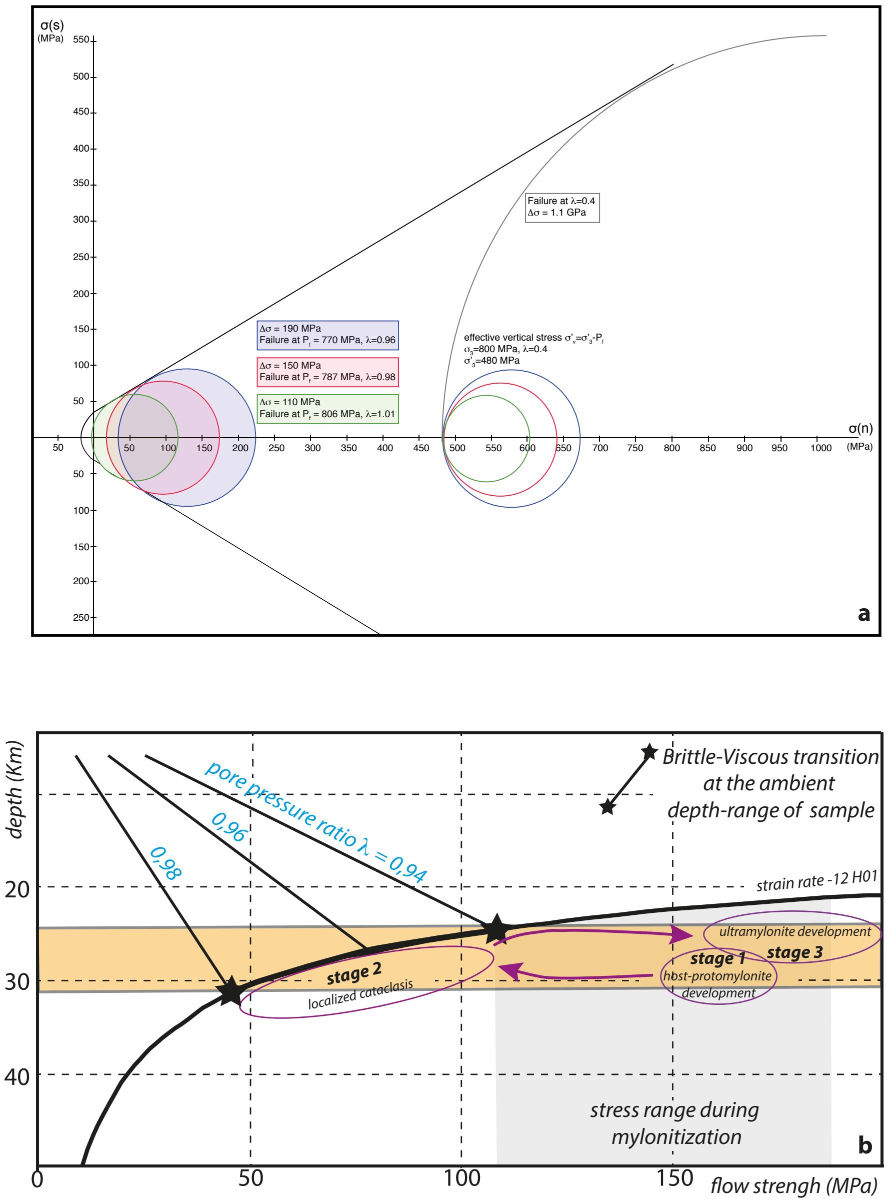

Fig.09

Solid Earth Discuss., doi:10.5194/se-2017-11, 2017
Manuscript under review for journal Solid Earth
Published: 7 February 2017

Solid Earth
Discussions
Open Access
EGU

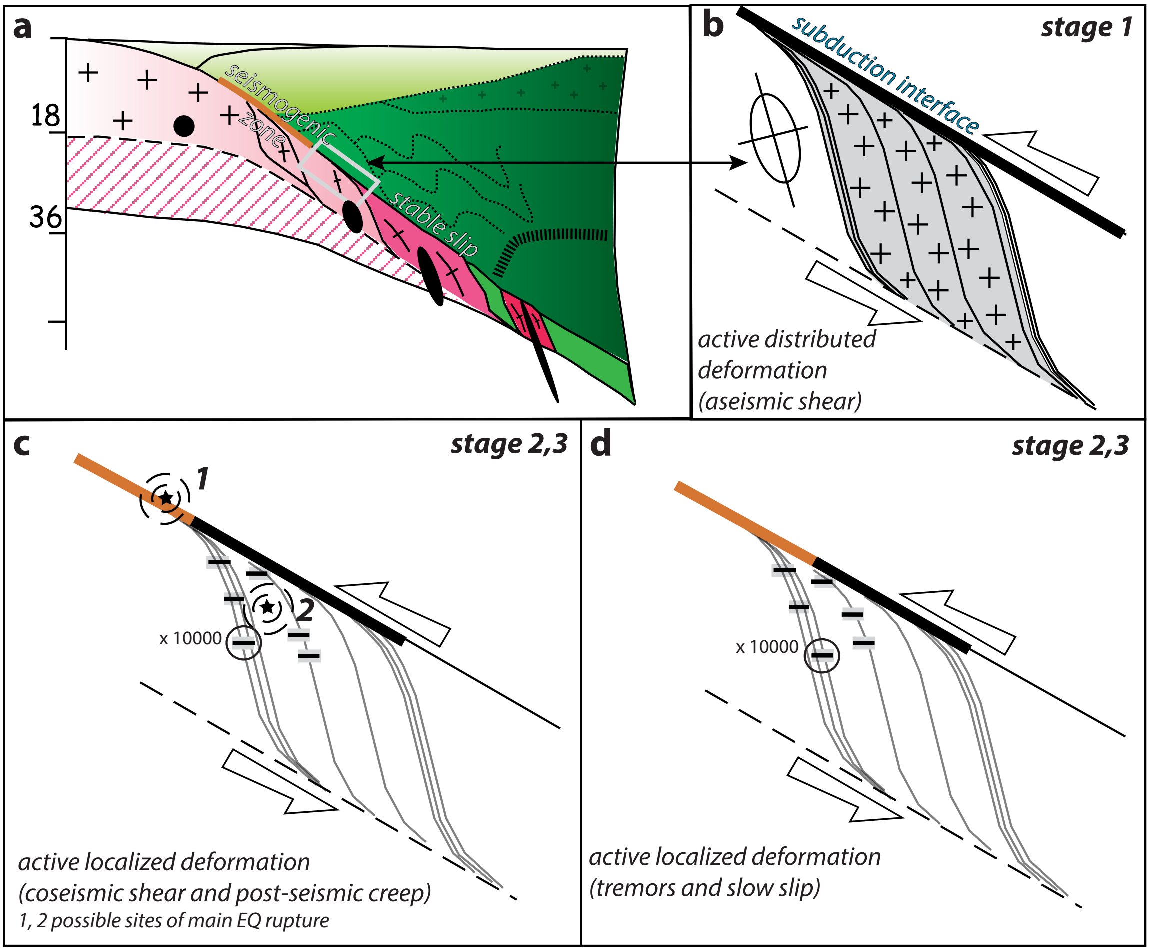

Fig.10

Solid Earth Discuss., doi:10.5194/se-2017-11, 2017
Manuscript under review for journal Solid Earth
Published: 7 February 2017

Solid Earth Discussions
Open Access

Amphibole	Am1	Am3	Am4	Am5	Am6N	Am6B	Am7
Wt%							
SiO2	51,58	51,30	50,62	50,97	50,28	50,61	52,62
TiO2	0,35	0,32	0,52	0,24	0,20	0,39	0,16
Al2O3	1,67	1,89	1,97	1,73	2,22	1,85	2,59
Cr2O3	0,00	0,00	0,00	0,00	0,00	0,00	0,00
FeO	28,13	29,65	28,80	28,77	30,25	30,18	27,94
MnO	0,00	0,15	0,00	0,20	0,00	0,00	0,00
MgO	2,24	1,86	1,97	2,16	1,64	1,98	1,90
CaO	0,06	0,05	0,10	0,09	0,13	0,14	0,06
Na2O	6,44	6,63	6,66	6,79	6,02	6,42	6,88
K2O	0,41	0,39	0,46	0,38	0,35	0,43	0,71
TOT	90,88	92,24	91,10	91,33	91,09	92,00	92,86
Cations							
Si	8,16	8,09	8,09	8,11	8,07	8,05	8,17
Al IV	0,00	0,00	0,00	0,00	0,00	0,00	0,00
Sum T	8,16	8,09	8,09	8,11	8,07	8,05	8,17
Al VI	0,31	0,35	0,37	0,32	0,42	0,35	0,47
Fe3+	1,70	1,56	1,42	1,54	1,46	1,50	1,45
Ti	0,04	0,04	0,06	0,03	0,02	0,05	0,02
Cr	0,00	0,00	0,00	0,00	0,00	0,00	0,00
Mg	0,53	0,44	0,47	0,51	0,39	0,47	0,44
Fe2+	2,02	2,35	2,43	2,28	2,61	2,51	2,18
Mn	0,00	0,02	0,00	0,03	0,00	0,00	0,00
Sum C	4,60	4,76	4,75	4,71	4,90	4,88	4,56
Mg	0,00	0,00	0,00	0,00	0,00	0,00	0,00
Mn	0,00	0,00	0,00	0,00	0,00	0,00	0,00
Fe2+	0,00	0,00	0,00	0,00	0,00	0,00	0,00
Ca	0,01	0,01	0,02	0,02	0,02	0,02	0,01
Na	1,97	1,99	1,98	1,98	1,87	1,98	1,99
Sum B	1,98	2,00	2,00	2,00	1,89	2,00	2,00
Na	0,00	0,04	0,08	0,11	0,00	0,00	0,08
K	0,08	0,08	0,09	0,08	0,07	0,09	0,14
Sum A	0,08	0,12	0,17	0,19	0,07	0,09	0,22
TOT	14,82	14,97	15,01	15,01	14,93	15,02	14,95

-: below detection limits

Stilpnomel:	Fill1	Fill2	Fill3	Fill4
Wt%				
SiO2	45,20	48,73	40,85	42,13
TiO2	0,13	0,07	0,30	0,18
Al2O3	21,19	12,22	17,08	20,28
Cr2O3	-	0,11	-	-
FeO	13,54	20,45	19,60	16,13
MnO	-	0,16	-	-
MgO	2,39	0,95	1,94	1,92
CaO	0,16	0,20	0,29	0,32
Na2O	0,16	1,00	0,37	0,26
K2O	4,68	3,00	5,05	4,89
TOT	87,45	86,89	85,48	86,11
Cations				
Si	7,418	8,292	7,235	7,200
Al vi	1,582	0,708	1,765	1,800
Sum Z	9,000	9,000	9,000	9,000
Al iv	2,516	1,743	1,800	2,284
Ti	0,016	0,009	0,040	0,023
Cr	0,000	0,015	0,000	0,000
Fe3+	0,000	0,000	0,000	0,000
Fe2+	1,858	2,909	2,902	2,304
Mn	0,000	0,023	0,000	0,000
	0,584	0,241	0,512	0,489
Sum Y	4,974	4,939	5,254	5,100
Ca	0,028	0,036	0,055	0,059
Na	0,051	0,330	0,127	0,086
K	0,979	0,651	1,141	1,066
Sum X	1,058	1,017	1,323	1,210
TOT	15,032	14,956	15,576	15,311

- : below detection limit

Feldspar	K-feld	K-feld	K-feld	K-feld	Albite	Albite	K-Feld	Albite	Albite	K-feld	Albite
Wt%											
SiO2	64,47	68,51	63,50	64,25	68,06	67,82	64,35	68,12	67,75	63,98	68,33
TiO2	-	-	-	-	-	-	0,02	-	-	-	0,07
Al2O3	18,75	20,33	18,32	18,66	20,50	19,84	18,28	19,43	20,20	18,91	20,43
Cr2O3	-	-	-	-	-	-	-	-	-	-	-
FeO	-	0,15	-	-	0,13	-	-	0,27	0,09	0,11	-
MnO	-	-	-	-	-	-	0,03	-	-	-	0,07
MgO	-	-	0,04	-	0,04	-	-	-	-	-	-
CaO	-	-	-	-	-	0,03	-	-	-	-	-
Na2O	2,44	0,18	0,17	0,19	11,03	11,44	-	11,31	11,56	0,20	11,17
K2O	13,48	9,05	16,32	14,72	0,28	0,05	15,74	0,16	0,04	14,39	0,56
TOT	99,14	98,22	98,35	97,82	100,04	99,18	98,42	99,29	99,64	97,59	100,63
Cations											
Si	11,92	12,25	11,95	12,02	11,88	11,93	12,03	11,99	11,88	11,98	11,88
Al	4,09	4,28	4,06	4,11	4,22	4,11	4,03	4,03	4,17	4,17	4,18
Sum Z	16,01	16,53	16,02	16,13	16,09	16,05	16,06	16,01	16,05	16,16	16,06
Fe3+	0,00	0,00	0,00	0,00	0,00	0,00	0,00	0,00	0,00	0,00	0,00
Fe2+	0,00	0,02	0,00	0,00	0,02	0,00	0,00	0,04	0,01	0,02	0,00
Mg	0,00	0,00	0,01	0,00	0,01	0,00	0,00	0,00	0,00	0,00	0,00
Ca	0,00	0,00	0,00	0,00	0,00	0,01	0,00	0,00	0,00	0,00	0,00
Na	0,87	0,06	0,06	0,07	3,73	3,90	0,00	3,86	3,93	0,07	3,76
K	3,18	2,06	3,92	3,51	0,06	0,01	3,75	0,04	0,01	3,44	0,12
Sum X	4,05	2,15	3,99	3,58	3,82	3,92	3,75	3,93	3,95	3,53	3,89
TOT	20,06	18,68	20,01	19,71	19,91	19,97	19,82	19,95	20,00	19,68	19,95
%Ab	21,58	2,93	1,56	1,92	98,36	99,57	0,00	99,08	99,77	2,07	96,81
%An	0,00	0,00	0,00	0,00	0,00	0,14	0,00	0,00	0,00	0,00	0,00
%Or	!"#$%	&!#'!	&"#$$	&"#'"	(#)$	'#%&	("#'	'#&%	'#%*	&!#&*	*#(&

tab 1